FBEC OFFICE FILE COPY

AFFDL-TR-75-96
ADA 018-860

THE FATIGUE CRACK PROPAGATION DELAY BEHAVIOR IN 2024-T3 ALUMINUM ALLOY DUE TO SINGLE OVERLOAD/UNDER-LOAD SEQUENCES

SCHOOL OF MECHANICAL ENGINEERING
PURDUE UNIVERSITY
WEST LAFAYETTE, INDIANA

AUGUST 1975

FINAL REPORT FOR PERIOD – JANUARY 1974 – JUNE 1975

Approved for public release; distribution unlimited

Best Available Copy

AIR FORCE FLIGHT DYNAMICS LABORATORY
Air Force Systems Command
Wright-Patterson Air Force Base, Ohio 45433

20060921118

NOTICE

When Government drawings, specifications, or other data are used for any purpose other than in connection with a definitely related Government procurement operation, the United States Government thereby incurs no responsibility nor any obligation whatsoever; and the fact that the Government may have formulated, furnished, or in any way supplied the said drawings, specifications, or other data, is not to be regarded by implication or otherwise as in any manner licensing the holder or any other person or corporation, or conveying any rights or permission to manufacture, use, or sell any patented invention that may in any way be related thereto.

This report has been reviewed by the Office of Information (OI) and is releasable to the National Technical Information Service (NTIS). At NTIS, it will be available to the general public, including foreign nations.

This technical report has been reviewed and is approved for publication.

J.P. Gallagher

J. P. GALLAGHER
Project Engineer
Fatigue, Fracture and Reliability Gp

R.M. Bader

ROBERT M. BADER, Chief
Structural Integrity Branch
Structures Division

FOR THE COMMANDER

Gerald G. Leigh

GERALD G. LEIGH, Lt Col, USAF
Chief, Structures Division

Copies of this report should not be returned unless return is required by security considerations, contractual obligations, or notice on a specific document.

SECURITY CLASSIFICATION OF THIS PAGE (When Data Entered)

REPORT DOCUMENTATION PAGE

READ INSTRUCTIONS BEFORE COMPLETING FORM

1. REPORT NUMBER AFFDL-TR-75-96	2. GOVT ACCESSION NO.	3. RECIPIENT'S CATALOG NUMBER
4. TITLE (and Subtitle) THE FATIGUE CRACK PROPAGATION DELAY BEHAVIOR IN 2024-T3 ALUMINUM ALLOY DUE TO SINGLE OVERLOAD/UNDERLOAD SEQUENCES		5. TYPE OF REPORT & PERIOD COVERED Final Technical Report 1 Jan 1974 - 30 June 1975 6. PERFORMING ORG. REPORT NUMBER
7. AUTHOR(s) B. M. Hillberry, Wm. X. Alzos and A. C. Skat, Jr.		8. CONTRACT OR GRANT NUMBER(s) F 33615-74-C-3056
9. PERFORMING ORGANIZATION NAME AND ADDRESS School of Mechanical Engineering Purdue University West Lafayette, Indiana 47907		10. PROGRAM ELEMENT, PROJECT, TASK AREA & WORK UNIT NUMBERS Project: 192901 Task: 19290105
11. CONTROLLING OFFICE NAME AND ADDRESS Air Force Flight Dynamics Laboratory Air Force Systems Command Wright-Patterson Air Force Base Ohio 45433		12. REPORT DATE August 1975 13. NUMBER OF PAGES
14. MONITORING AGENCY NAME & ADDRESS(if different from Controlling Office) Same		15. SECURITY CLASS. (of this report) UNCLASSIFIED 15a. DECLASSIFICATION/DOWNGRADING SCHEDULE

16. DISTRIBUTION STATEMENT (of this Report)

Approved for Public Release: Distribution Unlimited

17. DISTRIBUTION STATEMENT (of the abstract entered in Block 20, if different from Report)

18. SUPPLEMENTARY NOTES

19. KEY WORDS (Continue on reverse side if necessary and identify by block number)

Fatigue
Crack propagation
Overload
Underload
Delay
Residual stress intensity factor
Crack closure

20. ABSTRACT (Continue on reverse side if necessary and identify by block number)

The fatigue crack delay behavior due to single overload/underload sequences was studied in center crack panel specimens of 2024-T3 aluminum alloy. The applied loading consisted of constant amplitude loading, an applied overload immediately followed by an underload and then constant

DD FORM 1 JAN 73 1473 EDITION OF 1 NOV 65 IS OBSOLETE UNCLASSIFIED

SECURITY CLASSIFICATION OF THIS PAGE (When Data Entered)

20. amplitude loading at the pre-overload level. The tests were carried out at a quasi-constant stress intensity level by shedding the load to maintain the stress intensity level within three per cent.

The loading parameters investigated are the stress intensity ratios, overload level to maximum fatigue level, underload level to overload level, and minimum fatigue level to overload level. The magnitude of the overload level is the same for all test conditions. A three dimensional test matrix is used to systematically investigate the effects of each of the three test parameters. Crack length versus number of cycles recorded at 0.0004 in. increments of crack growth following the overload/underload sequence provides a very good representation of the growth rate behavior through the overload affected region. Using an inverse technique the maximum opening stress intensity is determined from the minimum growth rate data and the constant amplitude growth rate data. The results show that increasing the amount of underload decreases the number of delay cycles. Also, it is shown that the number of delay cycles is directly related to the minimum growth rate following the overload.

The concept of crack closure is extended to include the effects of the overload/underload sequence. From this the maximum value of the opening stress intensity level and the minimum growth rate are determined. This is used to predict the number of delay cycles.

FOREWORD

This report describes an investigation of the delay behavior on fatigue crack propagation resulting from overload/underload sequences performed under Air Force Contract F 33615-74-C-3056, Project 192901, Flight Vehicle Structures Research, Task 19290105, Residual Stress Intensity Factors. Technical monitor for the project was Dr. J. P. Gallagher (AFFDL/FBE). The project period was 2 Jan 74 to 30 June 75.

This program was conducted by the School of Mechanical Engineering, Purdue University, West Lafayette, Indiana. Principle Investigator for the program was Professor B. M. Hillberry; Graduate Research Assistants were Mr. Wm. X. Alzos and Mr. A. C. Skat, Jr. Material for the test samples were provided by the Aluminum Company of America. Other reports or publications resulting from the research performed under this contract are References 11, 22, 23, and 24 listed at the end of the report.

This report was submitted by the authors June 1975.

TABLE OF CONTENTS

LIST OF ILLUSTRATIONS

LIST OF TABLES

LIST OF SYMBOLS

A	constant
a	crack length
a_{OL}	crack length at which overload/underload cycle was applied
Δa^*	overload affected crack length
B	specimen thickness
b	constant
C_i	constants
$\frac{da}{dN}$	crack growth rate
K_{MAX}	maximum cyclic stress intensity
K_{MIN}	minimum cyclic stress intensity
K_{OL}	overload stress intensity
K_{UL}	underload stress intensity
K_{OP}	opening stress intensity
K_R	residual stress intensity
ΔK	stress intensity range, $K_{MAX} - K_{MIN}$
N	number of cycles
N_D	number of delay cycles
n	constant
Q_{OL}	ratio of K_{OL}/K_{MAX}
R_{EFF}	effective stress intensity ratio, $\frac{K_{MIN} - K_R}{K_{MAX} - K_R}$
R_F	stress intensity ratio, K_{MIN}/K_{MAX}
R_M	ratio of K_{MIN}/K_{OL}
R_{UO}	ratio of K_{UL}/K_{OL}

r_y calculated plastic zone radius

U $\dfrac{K_{MAX} - K_{OP}}{K_{MAX} - K_{MIN}}$

U_{OL} $\dfrac{K_{OL} - K_{OP}}{K_{OL} - K_{UL}}$

β constant

σ_{ys} yield strength of material

INTRODUCTION

The load interaction effects on fatigue crack propagation due to variable amplitude loading have been a subject of investigation for many years and will undoubtedly continue to be so for some time. The inability to adequately predict these interaction effects has prompted recent interest in studying the interaction due to simple load patterns and its influence on fatigue crack propagation. Of particular interest is the decrease in growth rate (delay effect or crack retardation) which normally follows a high overload or a reduction in the load level. This delay can have a significant influence on the fatigue life of a structure [1,2][1].

An understanding of the effect of load interactions, resulting from changes in the cyclic load level, on the fatigue crack propagation is desirable both in design and in the prevention of failure of components subjected to time varying load histories. Several studies have been undertaken to investigate the delay effect due to simple load patterns such as single and multiple overload/underload sequences [2-18]. Various explanations and models have been suggested for describing this delay behavior [2-21], however, it is still not entirely clear which parameters are significant.

Although reduction of the overload effect has been observed for subsequently applied underloads, a systematic study is needed for the definition and isolation of the associated variables. Such a study is essential before predictive models for fatigue crack growth can be used to adequately describe the influ-

[1] Numbers in brackets refer to references at end of report.

ence of such loadings. This study was undertaken to quantitatively investigate the fatigue crack delay or retardation effects of overstressing and understressing on an otherwise constant amplitude load cycling situation. By considering a three dimensional matrix representation of the selected experimental variables, each variable can be studied and its influence on the crack retardation phenomenon assessed. In addition to isolating the effects of the various parameters on the delay behavior, this study was also undertaken to determine if the effective stress parameters at the crack tip could be defined using an inverse technique. With this technique, the growth rate following the overload/underload sequence is measured. This measured growth rate is then used in the constant amplitude growth rate equation to determine an effective applied stress intensity.

Using the results of this investigation, an extended crack closure model is developed which accounts for all of the quantitative trends in the data, and also can be used to predict the crack opening stress intensity level and the number of delay cycles for a given set of test conditions. The crack closure phenomenon is interpreted as an effect, capable of quantifying retardation in crack growth, but caused by the presence of residual stresses in the vicinity of the crack tip.

Additional details of this study are contained in References 22-24.

EXPERIMENTAL INVESTIGATION

Selection of Variables and Development of Test Matrix

A test program was designed which isolated what were believed to be the relevant parameters affecting fatigue crack growth in the presence of single overload/underload cycles. An earlier observation [11] indicated an apparent difference in crack growth delay due to overloads which create plane stress conditions and overloads which create plane strain conditions. Therefore, K_{OL} was chosen such that the crack tip would be in a state of plane stress. A state of plane stress was assumed to exist if the plastic zone diameter, $2r_y$, due to the overload was greater than the thickness of the specimen, B, where

$$2r_y = \frac{1}{\pi}\left(\frac{K}{\sigma_{ys}}\right)^2 \tag{1}$$

For this study, the overload stress intensity level was chosen to be the same for all of the tests (K_{OL} = 33.33 ksi$\sqrt{\text{in}}$) which gave

$$2r_y = 0.109 > B = 0.100 \text{ in.} \tag{2}$$

Thus, all fatigue cracks for the tests performed were propagated to establish steady state conditions, overloaded into plane stress and returned to steady state loading.

The parameters chosen to be investigated were the stress intensity ratios: overload level to maximum fatigue level, $Q_{OL} = K_{OL}/K_{MAX}$; underload level to overload level, $R_{UO} = K_{UL}/K_{OL}$; and minimum fatigue level to overload level, $R_M = K_{MIN}/K_{OL}$. The overload/underload load sequence and the above parameters are illustrated in Figure 1. These parameters were believed to be the signifi-

cant loading parameters necessary to correlate the delay effects. By specifying the value of each of these ratios and one stress intensity level (in this study, K_{OL} was the same for all tests) the other test conditions, K_{MAX}, K_{MIN}, and K_{UL}, are established.

These values were selected because 1) R_{UO}, when isolated, would conveniently represent the effect accompanying underloading from the overload to the underload value, a key parameter for both residual stress and opening stress concepts; 2) Q_{OL} had already been shown to be an important parameter in the determination of the arrest/delay boundary by Probst [8] and Himmelein [11] and 3) R_M had been shown to be of importance in tests with overloads only [11]. In order that each parameter's effect on fatigue life be properly assessed, a three-dimensional test matrix was developed with R_{UO}, Q_{OL}, and R_M, forming the coordinate axes. Using such a scheme, lines parallel to each axis isolated a single variable and an analysis of the test results would yield information on how fatigue crack propagation was affected by that one variable. Two planes parallel to the coordinate planes were chosen for principal investigation: Q_{OL} vs. R_{UO} and R_M vs. R_{UO}, as shown in Figures 2 and 3. In addition, tests in a third plane which spanned the values of the Q_{OL} and R_M ratios used in the other two planes were run to assess the accuracy of the correlations. See Figure 4. It should be noted in Figures 2 and 3 that these two planes intersect at $Q_{OL} = 1.8$ and $R_M = 0.22$ and, therefore, the middle row of tests in each plane is the same set of tests.

Since correlation of the test results with opening stress and residual stress concepts determined from an inversion technique was desired, a primary objective in performing the tests was to obtain measured crack growth rates within the load interaction zone due to the overload. Therefore, precise data of crack length and number of cycles were required following the overload.

By choosing all of the tests to have the same overload level, the effect of varying the overload level was not investigated. The tests included in this study were chosen to study the principle effects of the selected parameters. In all tests the underload followed the overload with the exception of two tests, R-12 and R-13, (not shown in the matrix) which were run specifically to determine the effect of reversing the order of the overload/underload sequence.

Test Specimen and Material

The test specimens used in this study were cut from 2024-T3 aluminum alloy, 0.100 inch thick from the same stock as the specimens used in Ref. [11]. Using ASTM standard specimens, the material was determined to have the following tensile properties [11]:

Yield strength = 56.9 ksi

Ultimate Strength = 69.0 ksi

% Elongation = 14.2%

The geometry for the fatigue test specimen is shown in Figure 5. The stress raiser shown in detail in Figure 5 was machined with an electron-discharge technique. The specimens were obtained with a mill finish and were polished to a mirror finish in the vicinity of the crack path to facilitate optical observation of the crack tip during crack growth measurement. The loading was applied parallel to the direction of rolling of the material.

Test Equipment

The specimens were loaded in a 20 kip, closed-loop, electro-hydraulic test machine operated in load control. The feedback signal was continuously monitored with a specially designed readout which provided a digital display

of peak to peak, maximum, minimum or mean level of the cyclic signal. A counter, also connected to the feedback signal, was used to count the number of cycles following the overload during each test. This counter was attached directly to a printer which was used to record the number of cycles. A strobe synchronized with the input signal was used to illuminate the viewing surface of the test specimen.

The crack length was measured optically with a 100x microscope mounted on a two directional traversing system. A digital resolver system on the horizontal traverse produced a digital readout in the horizontal direction with a resolution of 0.001 mm (0.00004 in.). The direction of travel of the traverse was never changed during a test to eliminate any hysteresis effects in the system. The data were collected by advancing the microscope an increment distance (0.01 or 0.02 mm) and recording the number of cycles when the crack had advanced that increment. For the slower growth rates, $\frac{da}{dN} < 5 \times 10^{-6}$ in/cycle, the ability to observe the crack tip suggests an experimental error in the measurement of Δa to be in the order of $\pm$ 0.002 mm (0.00008 in.). At the faster growth rates, $\frac{da}{dN} > 5 \times 10^{-5}$, this may be in the order of $\pm$ 0.01 mm (0.0004 in.).

For very slow crack propagation rates, $\frac{da}{dN} \leq 5 \times 10^{-7}$ in/cycle, the number of cycles, N, was recorded every 0.01 mm (0.0004 in.) with all N values within an estimated interval of confidence of $\pm$ 50 cycles of the true value.

Lightweight aluminum compression guides lined with 1/8 in. felt were used to support the specimen when compressive underloads were applied. The guides were removed for subsequent cycling. The optical system is shown in Figure 6 and the guides, together with a specimen, are shown in Figure 7.

Test Procedure

Since the scope of this study strictly involved the effects of loading on fatigue crack propagation, care was taken to control as many other variables as possible. All tests were subject to nearly identical environmental conditions of dessicated air and room temperature. All fatigue cycling was done at 20 Hz except for tests 1, 2, and 3, which were cycled at rates of 10 Hz due to the rapid crack propagation for these tests. All overload and underload cycles were applied at 0.02 Hz.

In order to have a basis for comparison between tests in the test matrix, the stress intensity factors were held at quasi-constant values throughout each test by shedding the applied load. The applied load was reduced at every 5% increase in crack length. This insured that the actual K level was maintained between 0% and +3% of the desired values. The load levels were calculated according to Tada's modification of Fedderson's formula [25] for the stress intensity factor of a center cracked specimen. This is

$$P = \frac{K(2bt)}{\sqrt{\pi a}} \cdot \frac{1}{f(a/b)} \tag{3}$$

K = desired stress intensity factor ($\mathrm{ksi}\sqrt{\mathrm{in}}$)

t = thickness of specimen (in.)

a = one-half crack length (in.)

$2b$ = width of specimen (in.)

$f(a/b)$ = correction factor for specimen geometry

$$= [1 - .025(a/b)^2 + .06(a/b)^4]\sqrt{\sec\left(\frac{a}{2b}\right)}$$

To make certain that only single overload/underload effects were observed, care was taken in each test to establish equilibrium before the application of

the overload/underload sequence. The steady state condition prior to the overload was achieved by propagating the fatigue crack at least 6 mm (0.24 in.) (over twice the theoretical overload plastic zone diameter) at the quasi-constant stress intensity values specified for the test. The overload/underload sequence determined from Equation 3 using the measured crack length was then applied. Following this, cyclic loading was resumed at the pre-overload level with the load being shed in the same manner as described above to maintain the quasi-constant loading. The crack length, a, at the point of the overload application varied between 0.27 mm and 2.03 mm (0.41 to 2.03 in.). The corresponding overload net section stress varied between 0.27 and 0.55 of the yield strength of the material.

Cycling was continuous for both pre-overload and post-overload fatigue cycling to negate the possibility of time or underloading to zero load affecting subsequent crack growth.

The crack length, a, and number of cycles, N, were monitored continuously for each test and discrete data points collected every 0.01 mm, 0.02 mm, or 0.05 mm (0.0004, 0.0008 or 0.002 in.), the larger intervals used for more rapid crack propagation rates. Data were recorded by advancing the optical system by the specified increment and pressing a trigger button to the printer (monitoring number of cycles) when the crack had grown to the incremented position. Typical fracture surfaces are shown for three specimens in Figure 8.

DATA REDUCTION - NUMERICAL DIFFERENTIATION

One of the objectives of this study was to characterize the growth rate behavior through the overload affected zone following the overload/underload sequence. To obtain the growth rate, da/dN, it was necessary to record sufficient a versus N data and then differentiate these data. Several different techniques have been used for the numerical differentiation of experimental data. Incremental differentiation methods tend to amplify any small scale variation in the actual data. As an alternative, a spline function method was selected in which a series of cubic polynomials were fit to the experimental data and then analytically differentiated to obtain the crack growth rate. This method, frequently used to differentiate experimental data [26,27], provides a smoothed crack growth rate curve.

To apply the spline method, third order polynomials were fit to three intervals of the entire post-overload a versus N data of a given test. The values of the polynomials and their first two derivatives were matched at the knots (points where the polynomials join). The computer technique of de Boor and Rice [28,29] was modified to allow the first interior knot to be fixed at a specified position. This first knot was located after the intial deceleration where the a versus N curve started to level out. It was found for all tests that this knot could be located at a point equal to 5 per cent of the calculated plastic zone diameter. The computer routine then optimally located the second knot and determined the coefficients of the three polynomials which minimized the least square error over the entire range of the data.

Figure 9 shows a typical fit of the spline function to the a versus N data and Figure 10 shows the corresponding analytically differentiated curve,

i.e., $\frac{da}{dN}$ versus a. The spline method of differentiation was compared to a linear, seven point least squares movable strip method [2,30]. The resulting growth rate from this method is also shown in Figure 10 for the same data. To compare the two methods, the da/dN from the movable strip method was numerically integrated and compared with the original data. This is shown in Figure 9. With the spline method, integration of da/dN will simply reproduce the original spline function since the derivative is obtained analytically. As can be seen from Figure 9 and 10, the spline method provides a good representation of the a versus N data and a smoothed da/dN curve. An analytical expression is also obtained for an entire data set. It should be pointed out that with the movable strip technique a considerably smoother differentiation than that shown can be obtained by using a wider strip (either by increasing the number of data points or by using only every third or fourth data point).

One of the important characteristics of the delay behavior is the minimum growth rate following the overload. Therefore, the minimum growth rate for each test as determined from the spline method was compared with the data graphically. In some of the tests the spline method produced a slightly lower value for the minimum growth rate. For these tests (numbers 3, 10, 17, 23, 32, 33, 34) the graphical values were used.

TEST RESULTS

Constant Amplitude Tests

For the purpose of comparing the fatigue crack growth rates obtained from the actual test data, two constant stress amplitude tests were performed at each of five different fatigue stress ratios: $R_F = 0.01, 0.2, 0.33, 0.44, 0.55$. By performing constant stress amplitude tests, the value of the stress intensity factors (K_{MAX}, K_{MIN}) increased with increasing crack length, while R_F was constant. By measuring crack length and the number of cycles, the crack growth rate could be determined for a given value of ΔK and corresponding R_F. The results are shown in Figure 11.

A series of three cubic splines [28,29] were fit to each set of a vs. N (approximately 85 points per set) with the two interior knot positions optimized so as to minimize the least square error. The values of da/dN were obtained by differentiating the resulting spline functions. With a knowledge of the loads, P_{MAX} and P_{MIN}, as well as the crack length and number of cycles as represented by the spline function, the values of ΔK_{EFF} and the corresponding growth rate were determined at 170 points for each test, yielding a total of 1700 points for all ten tests. From these values of da/dN and ΔK_{EFF}, the values of the two constants for the steady state growth rate equations were determined using a least square fit. This gave for Elber's equation [19,20]

$$\frac{da}{dN} = C(\Delta K_{EFF})^n \tag{4}$$

$$\Delta K_{EFF} = (0.5 + 0.4R_F)\Delta K$$

$$C = 6.92 \times 10^{-9}$$

$$n = 3.86$$

The data were also shown to agree with Gallagher's equation [31]

$$\frac{da}{dN} = A[\Delta K(1 + \beta R_F)]^b \tag{5}$$

where
$\beta = 0.698$ for $R_F > 0$

$\beta = 0.418$ for $R_F < 0$

$A = 6.78 \times 10^{-10}$

$b = 3.58$

The constants in this equation were determined by Gallagher [31] using Hudson's data [32].[1]

Equation 4 was used in determining the experimental parameters associated with extended crack closure and Equation 5 was used in calculating the residual stress intensity parameters. These concepts are discussed in detail later.

Overload/Underload Tests

A summary of the test conditions and results for all of the overload/underload tests is presented in Table I. The actual loading conditions for each of the tests in the three planes of the original test matrix are shown in Figures 2-4.

Following the completion of the test program as presented, three additional tests were run in order to better define crack growth trends for tests having negative R_{UO} and high Q_{OL} values, which were the two parameters found to be of most significance in determining the amount of delay. These tests (16-2.4, 17-2.4, and 16-2.6) are in the same Q_{OL} vs. R_{UO} plane as the original matrix tests shown in Figure 2. To better define an arrest/delay boundary for

[1] Using Gallagher's form of the growth equation a minimum least squared error was obtained for the data of this study with $A = 6.28 \times 10^{-10}$, $b = 3.79$, and $\beta = 0.647$ (for $R_F > 0$ only).

negative R_{UO} values, three additional tests were run with $Q_{OL} = 3.0$.

The data obtained from the tests in the matrices illustrate the same qualitative trends as noted by other investigators. By representing the a vs. N data from each of the tests with the spline functions, the results can be illustrated by plotting the resulting spline functions. These results are shown in matrix form in Figures 12 and 13 for the two principle planes. Analytical differentiation of the spline functions yields the corresponding da/dN vs. a curves shown in Figures 14 and 15.

The effects of varying each of the selected parameters (Q_{OL}, R_{UO}, or R_M) with all other parameters held constant can easily be compared in these figures. Horizontal directions from left to right on each of the matrices correspond to an increase in R_{UO} from a value of -1.00 to a value at which there is no applied underload. From the results, it is seen that as R_{UO} is increased, that is, as the underload value approaches the minimum stress intensity value, an increasing amount of crack delay results. Furthermore, it may be seen from the two matrices showing the growth rates of each test (Figures 14 and 15) that as R_{UO} increases, the minimum growth rate decreases. The number of delay cycles, N_D, and the minimum growth rate, $\left.\frac{da}{dN}\right|_{MIN}$, for each test are shown in matrix form in Figures 16 and 17. Consideration of vertical lines in Figure 16 yields information accompanying the variation of the parameter Q_{OL} for all other parameters held constant. The five vertical lines illustrate that as Q_{OL} increases, or as the value of K_{MAX} decreases for other stress intensity levels fixed, the number of delay cycles increases, with a corresponding decrease in the minimum growth rate. Examination of the vertical lines of the R_M vs. R_{UO} matrix (Figure 17) does not illustrate as significant a trend due to varying R_M as is observed for varying R_{UO} or Q_{OL}.

These observations suggest that R_M is of secondary importance in the prediction of delay as compared with the significant effect due to R_{UO} and Q_{OL}.

Efforts to correlate the measured overload affected zone, Δa^*, with the selected set of parameters did not yield any consistent trends. However, the average value of Δa^* was 0.104 in. (with a standard deviation of 0.029) which agrees reasonably well with the overload plastic zone diameter of 0.109 in. determined from Equation 1. This agreement between the calculated overload plastic zone size and the test data is in contradiction to the findings of Lankford and Davidson [14] who showed through the use of electron channeling patterns that fatigue crack retardation is not related to the maximum plastic zone dimension. However, it should be mentioned that since K_{OL} was the same for all tests, a range of overload plastic zone sizes was not considered in this study. The actual values of the measured delay zones, Δa^*, were determined from enlarged plots of the a vs. N data. The ratio of Δa^* to the plane stress plastic zone size, $2r_y$, ($2r_y$ = 0.109 in.) is shown for each of the original matrix tests (Figures 2 and 3) in Figure 18.

Tests R-12 and R-13 were run with the identical test conditions as tests 12 and 13 except the underload preceded the overload. N_D for these two reversed tests were 160,000 and 169,000 cycles respectively as compared to 14,400 and 42,600 cycles for tests 12 and 13 respectively. Test 15 had the same load levels except with no underload applied (K_{OL}, K_{MAX} and K_{MIN} were the same). N_D for this test was 142,000 cycles which compares favorably with N_D for the two reversed tests. This comparison indicates that an underload preceding an overload has a different effect than when the underload follows the overload. Also, it suggests that if an overload follows the underload, the overload essentially eliminates any effect due to the underload. Note that this is based only on the results of two tests and should be examined further.

INVERSE METHOD OF DETERMINING
CRACK TIP STRESS INTENSITY PARAMETERS

James and Anderson [33] used fatigue crack growth rate data and an inverse method to determine the stress intensity factor for a complex geometry. For their method, the constant amplitude growth rate was determined as a function of the applied K for a given material using a geometry for which the stress intensity factor was known. The fatigue crack growth rate in the complex specimen, made of the same material, was then measured. The applied K which produced this same growth rate in the known specimen is then the stress intensity factor (at the measured crack length) for the complex geometry.

A similar inverse approach was used in this study to evaluate the change in the effective stress intensity parameters at the crack tip resulting from the overload/underload sequence. Furthermore, it was possible to determine how these parameters changed throughout the overload affected zone. The inverse method involved experimentally determining the fatigue crack growth rate through the overload affected zone and then determining the effective applied stress intensity level from the constant amplitude growth rate equation. This is described further below.

Residual Stress Intensity Parameters

The minimum value of an effective residual stress intensity parameter was determined for each of the tests as described below. Using the following form of the constant amplitude growth rate equation

$$\frac{da}{dN} = A[(1 + \beta R)\Delta K]^b \tag{5}$$

and solving for R gives

$$R = \frac{1}{\beta} \left\{ \frac{1}{\Delta K} \left(\frac{1}{A} \cdot \frac{da}{dN} \right)^{\frac{1}{b}} - 1 \right\} \tag{6}$$

The effect of a residual stress ahead of the crack created by the overload/underload sequence would be to change the maximum and minimum values of the applied stress intensity levels by the amount of the effective residual stress, K_R, [31]. If the residual stress is compressive, then the effective value of the stress ratio, R_{EFF} would be

$$R_{EFF} = \frac{K_{MIN} - K_R}{K_{MAX} - K_R} \tag{7}$$

Solving for K_R gives

$$K_R = \frac{K_{MIN} - R_{EFF}\, K_{MAX}}{1 - R_{EFF}} \tag{8}$$

At the minimum growth rate following the overload/underload sequence, R_{EFF} will be a minimum. Therefore, K_R^{MAX} becomes

$$K_R^{MAX} = \frac{K_{MIN} - R_{EFF}^{MIN}\, K_{MAX}}{1 - R_{EFF}^{MIN}} \tag{9}$$

At this minimum growth rate, R_{EFF}^{MIN} can be determined from Equation 6 and the experimental results. This gives

$$R_{EFF}^{MIN} = \frac{1}{\beta} \left\{ \frac{1}{\Delta K} \left(\frac{1}{A} \cdot \left. \frac{da}{dN} \right|_{MIN} \right)^{\frac{1}{b}} - 1 \right\} \tag{10}$$

where $\left.\frac{da}{dN}\right|_{MIN}$ is the minimum growth rate determined from the test results and ΔK is the applied stress intensity range following the overload. Using $\left.\frac{da}{dN}\right|_{MIN}$ from the experimental results as given in Table I, R_{EFF}^{MIN} was determined for each of the tests using Equation 10. The corresponding values for K_R^{MAX} were determined using Equation 8 where K_R is a compressive residual stress. These results are presented in Table II.

It should be noted that R_{EFF} in Table II varies from -1.51 to +0.65 with most of the values being negative. These values were obtained using the inverse method and the constant amplitude growth rate equation, Equation 5, however, the value of β for negative R ratios in this equation is based on a limited amount of data.

It has been shown that the significant parameters associated with the Wheeler and Willenborg models are the parameters, K_{OL}/K_{MAX} and $K_{OL} - K_{MAX}$ respectively [13,18]. Attempts to correlate the residual stress intensity parameter K_R^{MAX} with these parameters yielded no apparent correlation. See Figures 19 and 20. This was anticipated since neither of these models account for the effect of changing the level of the underload. In this study, a significant effect resulted from changing the underload level.

Crack Opening Stress Intensity Parameters

According to Elber's crack closure theory [19,20], a fatigue crack remains closed during a portion of the tensile part of the load cycle. The effective stress intensity range, ΔK_{EFF}, that causes crack propagation is then

$$\Delta K_{EFF} = K_{MAX} - K_{OP} \tag{11}$$

where K_{OP} is the stress intensity level at which the crack opens. Elber's crack growth equation is then

$$\frac{da}{dN} = C(\Delta K_{EFF})^n \tag{4}$$

Substituting Equation 11 into Equation 4 and solving for K_{OP} gives

$$K_{OP} = K_{MAX} - \left(\frac{1}{C} \cdot \frac{da}{dN}\right)^{\frac{1}{n}} \tag{12}$$

Using the inverse method described above, K_{OP} following the overload/underload sequence can be found, since K_{MAX} is constant after the overload/underload and da/dN was measured. da/dN through the overload affected zone was determined from the spline function representation of the a versus N data. Using this, K_{OP} was determined through the overload affected zone for each of the tests in the two principle planes of the test matrix. These results are shown in Figures 21 and 22.

Also, the maximum value of K_{OP} was determined from

$$K_{OP}^{MAX} = K_{MAX} - \left(\frac{1}{C} \cdot \left.\frac{da}{dN}\right|_{MIN}\right)^{\frac{1}{n}} \tag{13}$$

where the minimum growth rate used in this equation is the value given in Table I. These results are given in Table III.

EXTENSION OF CRACK CLOSURE

Elber's crack closure concept [19,20] has been used to qualitatively explain the delay behavior following an overload condition [5,21]. In comparing the effective opening stress intensity factor following the overload/underload sequence with the constant amplitude behavior it is assumed that the overload/underload sequence establishes the residual stress field in the vicinity of the crack tip and that subsequent fatigue cycling does not change this stress field. Also, it is hypothesized that the resulting crack closure behavior is due to this residual stress field.

From crack closure, the effective stress intensity factor is

$$\Delta K_{EFF} = K_{MAX} - K_{OP} \tag{11}$$

and

$$\frac{da}{dN} = C(K_{MAX} - K_{OP})^n \tag{14}$$

For constant amplitude loading, Elber defined

$$U = \frac{K_{MAX} - K_{OP}}{K_{MAX} - K_{MIN}} \tag{15}$$

and found for 2024-T3 aluminum alloy

$$U = 0.5 + 0.4\ R_F \tag{16}$$

From the assumption that the overload/underload sequence establishes the residual stress field, U for the overload/underload sequence can be defined analogous to Equation 15 as

$$U_{OL} = \frac{K_{OL} - K_{OP}^{MAX}}{K_{OL} - K_{UL}} \quad (17)$$

As described in the previous section K_{OP}^{MAX} was determined using the experimentally determined minimum growth rate and, therefore, U_{OL} given by this equation also corresponds to the value at the minimum growth rate. If crack closure, as presented for constant amplitude loading, describes the results, then analogous to Equation 16

$$U_{OL}^{E} = 0.5 + 0.4R_{UO} \quad (18)$$

should agree with the experimentally determined values for U_{OL}. This is compared in Figure 23 which shows that Equation 18 does not adequately describe the results. However, it is apparent that U_{OL} is related to the loading conditions, i.e.,

$$U_{OL} = f(R_M, Q_{OL}, K_{OL}, \ldots) \quad (19)$$

Examination of the data suggested that this function should be of the form,

$$U_{OL} = C_1 + C_2R_{UO} + C_3R_{UO}^2 + C_4Q_{OL} \quad (20)$$

Using the results from the tests that did not arrest, a multiple linear regression analysis was performed to determine the constants of Equation 20.

$$\begin{aligned} C_1 &= 0.408 \\ C_2 &= 0.367 \\ C_3 &= 0.117 \\ C_4 &= 0.075 \end{aligned} \quad (21)$$

This equation can be compared with the experimental results by plotting $(U_{OL} - C_4Q_{OL})$ versus R_{UO}. This is seen to agree very well with the test results in Figure 24.

The influence of R_M was also examined by writing Equation 20 as

$$U_{OL} = C_1 + C_2R_{UO} + C_3R_{UO}^2 + C_4Q_{OL} + C_5R_M \qquad (22)$$

and performing the regression analysis. Although this provided a slight improvement in the results, an analysis of variance showed that the R_M parameter when included in this equation was not statistically significant. A similar analysis eliminating the Q_{OL} term in Equation 20 showed that Q_{OL} was statistically significant.

By combining Equation 17 with Equation 20 and solving for K_{OP}^{MAX} gives

$$K_{OP}^{MAX} = K_{OL}\ [1 - (1 - R_{UO})(C_1 + C_2R_{UO} + C_3R_{UO}^2 + C_4Q_{OL})] \qquad (23)$$

The values for K_{OP}^{MAX} calculated from this equation are compared with the experimentally determined values in Figure 25. As can be seen, the maximum opening stress intensity value is predicted almost exclusively within 5% of the measured value. Calculating K_{OP}^{MAX} from Equation 23 and using the growth rate equation, Equation 14, the minimum growth rates following the overload/underload sequences were determined. These results are compared with the experimental results in Figure 26. The calculated and experimental results for the extended crack closure parameters are presented in Table III.

The effects of the test parameters on the minimum growth rate can be more readily illustrated by substituting K_{OP}^{MAX} from Equation 23 into Equation 14 and

plotting the results from constant values of $\left.\frac{da}{dN}\right|_{MIN}$. Figure 27 shows several level curves of constant $\left.\frac{da}{dN}\right|_{MIN}$ as functions of Q_{OL} and R_{UO}. In this study if the growth was less than 0.0004 in. in 10^6 cycles, the test was stopped and the crack was assumed to have arrested. Therefore, a minimum growth rate of 4×10^{-10} in/cycle, which is the experimental resolution from the data, can be considered arrest. This is the curve labeled arrest in Figure 27. This arrest/delay boundary was based on the finite growth test results, however, it compares favorably with the experimentally determined arrest/delay boundary found by Himmelein [11] which was for overloads with no underload ($R_{UO} = R_M$). The arrest tests from this study are shown in Figure 27. The arrest/delay boundary from Elber's crack closure equation is also shown in this figure.

In evaluating the validity of the extended crack closure results, it is important to keep in mind the number of tests and the distribution of the loading conditions of these tests. Of the twenty-four tests used in determining the coefficients of Equation 20, only three tests had $Q_{OL} = 2.2$. Furthermore, eleven of the tests were performed in the small region of $0 \leq R_{UO} \leq 0.3$ and $1.6 \leq Q_{OL} \leq 1.8$. Even with this very unequal distribution of the data, the predicted results agree reasonably well with the actual data.

CORRELATION OF THE NUMBER OF DELAY CYCLES

There are a large number of parameters that influence the delay behavior resulting from a change in load level or load sequence. In this study only the simple overload/underload sequence was investigated. For these results it was shown that the maximum opening stress intensity can be correlated with the two parameters Q_{OL} and R_{UO}. This extension of crack closure can also be used to correlate the number of delay cycles with the observed results.

From the experimental results it was observed that the number of delay cycles, N_D, was directly related to the minimum growth rate, $\left.\frac{da}{dN}\right|_{MIN}$. This correlation is shown in Figure 28. From Equation 13

$$\left.\frac{da}{dN}\right|_{MIN} = C(K_{MAX} - K_{OP}^{MAX})^n \tag{24}$$

and the correlation of Figure 28 indicated that an average growth rate, $\frac{2r_y}{N_D}$, would correlate with $K_{MAX} - K_{OP}^{MAX}$, i.e.,

$$\frac{2r_y}{N_D} = A'(K_{MAX} - K_{OP}^{MAX})^{b'} \tag{25}$$

where

$$2r_y = \frac{1}{\pi}\left(\frac{K_{OL}}{\sigma_y}\right)^2$$

$$K_{MAX} - K_{OP}^{MAX} = \Delta K_{EFF}^{MIN}$$

A' and b' were found using a least squares fit on logarithmic coordinates,

$$A' = 8.17 \times 10^{-8}$$

$$b' = 2.82$$

Solving Equation 25 for N_D and substituting in for K_{OP}^{MAX} from Equation 23 gives

$$N_D = \frac{2r_y}{A'}\left\{K_{OL}\left[\frac{1}{Q_{OL}} - [1 - (1 - R_{UO})(C_1 + C_2R_{UO} + C_3R_{UO}^2 + C_4Q_{OL})]\right]\right\}^{-b'} \quad (26)$$

The values of N_D calculated from this equation are compared to the experimental values in Figure 29. As can be seen this shows good correlation.

It should be noted that $2r_y$ was the same for all tests in this investigation, however, Probst [8] also showed that a similar effective stress parameter correlated with the average growth rate.

It is interesting to note that the influence of the load level can be seen from Equation 26. By substituting in the expression for r_y and rewriting this equation gives

$$N_D \propto K_{OL}^{2-b'}[f(Q_{OL}, R_{UO}, R_M)]^{-b'} \quad (27)$$

Since $f(Q_{OL}, R_{UO}, R_M)$ is a function of non-dimensional parameters, the load level dependency is described entirely by the K_{OL} term in Equation 27. The value of b' is 2.82 and, therefore, the number of delay cycles is proportional to K_{OL} raised to the -0.82 power, i.e.,

$$N_D \propto K_{OL}^{-.82} \quad (28)$$

This indicates a minor dependency on the magnitude of the load level and that the ratios of the load levels are more significant. This substantiates the

work of Himmelein [11] who randomized load levels, but systematically varied the load ratios.

CONCLUSIONS

From the results of this study the following conclusions are made:

1) Utilizing a three dimensional test matrix, the delay effects due to each of the non-dimensional load parameters, Q_{OL}, R_{UO}, and R_M could be observed.

2) By carefully measuring the crack growth rate through the overload affected zone, the inverse method can be used to determine the crack tip stress parameters. This provides an effective method for studying the delay behavior.

3) Utilizing the crack tip stress parameters, it was found that the loading parameters Q_{OL} and R_{UO} had a significant effect on the delay behavior, the magnitude of the load pattern was of secondary importance and the influence of R_M was insignificant.

4) Comparing the results of two reversed tests in which the underload preceded the overload showed that the subsequent overload apparently eliminates any change in growth rate behavior due to the underload.

5) The number of delay cycles was found to correlate directly with the minimum growth rate following the overload/underload sequence.

6) An extension of the crack closure concept was developed which quantitatively describes the delay behavior following the overload/underload sequence. From this the maximum value of the opening stress intensity and the minimum growth rate following the overload/underload can be determined. The number of delay cycles can also be predicted.

REFERENCES

1. Schijve, J., "The Prediction of Fatigue Crack Propagation Under Service Load-Time Histories," NLR MP 73016U, National Aerospace Laboratory NLR, The Netherlands, 1973.

2. Gallagher, J. P., and Stalnaker, H. D., "Methods for Analyzing Fatigue Crack Growth Rate Behavior Associated with Flight by Flight Loading," Paper No. 74-367, Am. Inst. Aero. and Astro., April 1974.

3. Von Euw, E. F. J., Roberts, R. and Hertzberg, R. W., "Delay Effects in Fatigue Crack Propagation," Stress Analysis and Growth of Cracks, Proceedings of the 1971 National Symposium on Fracture Mechanics, Part 1. ASTM STP 513, pp. 230-259, Am. Soc. Test. and Mat., 1972.

4. Gardner, F. H., and Stephens, R. I., "Subcritical Crack Growth Under Single and Multiple Periodic Overloads in Cold-Rolled Steel," presented at Seventh National Symposium on Fracture Mechanics, University of Maryland, 1973.

5. Trebules, V. W., Roberts, R., and Hertzberg, R. W., "Effects of Multiple Overloads on Fatigue Crack Propagation in 2024-T3 Aluminum Alloy," Progress in Flaw Growth and Fracture Toughness Testing ASTM STP 536, pp. 115-146, Am. Soc. Test. and Mat., 1973.

6. Wei, R. P., Shih, T. T., and Fitzgerald, J. H., "Load Interaction Effects on Fatigue Crack Growth in Ti-6Al-4V Titanium Alloy," NASA CR2239, Nat. Aero. and Space Adm., 1973.

7. Corbly, D. M., and Packman, P. F., "On the Influence of Single and Multiple Peak Overloads on Fatigue Crack Propagation in 7075-T6511 Aluminum," Journal of Engineering Fracture Mechanics, Vol. 5, pp. 479-497, 1973.

8. Probst, E. P., and Hillberry, B. M., "Fatigue Crack Delay and Arrest Due to Single Peak Tensile Overloads," Am. Inst. Aero. and Astro. Journal, 12:3, pp. 330-335, March 1974.

9. Gallagher, J. P., "A Generalized Development of Yield Zone Models," AFFDL-TM-FBR-74-28, Air Force Flight Dynamics Laboratory, Wright Patterson Air Force Base, Ohio, January 1974.

10. Wei, R. P., and Shih, T. T., "Delay in Fatigue Crack Growth," International Journal of Fracture Mechanics, Vol. 10, pp. 77-85, 1974.

11. Himmelein, M. K. and Hillberry, B. M., "The Effect of Stress Ratio and Overload Ratio on Fatigue Crack Delay and Arrest Behavior Due to Single Peak Overloads," Proceedings Eighth National Symposium on Fracture Mechanics (1974) ASTM STP 590, Am. Soc. Test. and Mat., in print.

12. Hsu, T. M., and Lassiter, L. W., "Effects of Compressive Overloads on Fatigue Crack Growth," Paper No. 74-365, Am. Inst. Aero. and Astro., April 1974.

13. Petrak, G. J., and Gallagher, J. P., "Predictions of the Effects of Yield Strength on Fatigue Crack Growth Retardation in HP-9Ni-4Co-30C Steel," Journal of Engineering Materials and Technology, Am. Soc. Mech. Engr., in press.

14. Lankford, J., and Davidson, D. L., "Fatigue Crack Tip Plasticity Associated with Overloads and Subsequent Cycling," Southwest Research Institute, San Antonio, Texas, 1974.

15. Porter, R., "Method of Analysis and Prediction for Variable Amplitude Fatigue Crack Growth," Journal of Engineering Fracture Mechanics, Vol. 4, pp. 717-736, 1972.

16. Wheeler, O. E., "Spectrum Loading and Crack Growth," Journal of Basic Engineering, Trans. Am. Soc. Mech. Engr., 94:1, pp. 181-186, 1972.

17. Willenborg, J., Engle, R. M., and Wood, H. A., "A Crack Growth Retardation Model Using an Effective Stress Concept," AFFDL-TM 71-1-FBR, Air Force Flight Dynamics Laboratory, Wright-Patterson Air Force Base, Ohio, 1971.

18. Gray, T. D., and Gallagher, J. P., "Predicting Fatigue Crack Retardation Following a Single Overload Using a Modified Wheeler Model," Proceedings of Eighth National Symposium on Fracture Mechanics, 1974, ASTM STP 590, Am. Soc. Test. and Mat., in print.

19. Elber, W., "Fatigue Crack Closure Under Cyclic Tension," Journal of Engineering Fracture Mechanics, Vol. 2, pp. 37-45, 1970.

20. Elber, W., "The Significance of Fatigue Crack Closure," Damage Tolerance in Air Craft Structures, ASTM STP 486, pp. 230-242, Am. Soc. Test. and Mat., 1971.

21. Newman, J. C., "Finite Element Analysis of Fatigue Crack Propagation - Including the Effects on Crack Closure," Ph.D., Dissertation, Virginia Polytechnic Institute and State University, 1974.

22. Alzos, Wm. X., "The Effects of Single Overload/Underload Cycles on Fatigue Crack Propagation," M.S. Thesis, Purdue University, May, 1975.

23. Skat, A. C., Jr., "Evaluation of Extended Crack Closure in Fatigue Crack Delay Prediction for Single Overload/Underload Sequences," M.S. Thesis, Purdue University, May, 1975.

24. Alzos, Wm. X., Skat, A. C., Jr. and Hillberry, B. M., "An Extension of Crack Closure and the Effect of Single Overload/Underload Cycles on Fatigue Crack Propagation," presented at Symposium on Fatigue Crack Growth Under Spectrum Loads, Annual Meeting, Am. Soc. Test. and Mat., Montreal, Canada, June 1975.

25. Tada, H., Paris, P., and Irwin, G., The Stress Analysis of Cracks Handbook, Del Research Corporation, Hellerton, Pennsylvania, 1973.

26. Wold, S., "Spline Functions in Data Analysis," Research Group for Chemometrics, Institute of Chemistry, Umea University, S 901 87, Umea, Sweden.

27. Ahlberg, J. H., Nilson, E. N., and Walsh, J. L., The Theory of Splines and Their Applications, Academic Press, New York, 1967.

28. de Boor, C., and Rice, J. R., "Least Squares Cubic Spline Approximation I-Fixed Knots," Purdue University Computing Center Publication, 1968.

29. de Boor, C., and Rice, J. R., "Least Squares Cubic Spline Application II-Variable Knots," Purdue University Computing Center Publication, 1968.

30. Clark, W. G., Jr., and Hudak, S. J., "Variability in Fatigue Crack Growth Rate Testing," ASTM E-24.04.01 Task Group Report, Am. Soc. Test. and Mat., September 18, 1974.

31. Gallagher, J. P., Air Force Flight Dynamics Laboratory/FBRC, Wright-Patterson Air Force Base, Ohio, Private Communication, 1974.

32. Hudson, M. C., "Effect of Stress Ratio on Fatigue Crack Growth in 7075-T6 and 2024-T3 Aluminum Alloy Specimens," NASA TN D-5390, Nat. Aero. and Space Adm., 1969.

33. James, L. A., and Anderson, W. E., "A Simple Experimental Procedure for Stress Intensity Factor Calibration," Journal of Engineering Fracture Mechanics, Vol. 1, pp. 565-568, 1963.

TABLE I

TEST RESULTS

Test No.	K_{MAX} (ksi$\sqrt{in}$)	ΔK (ksi$\sqrt{in}$)	R_F	Q_{OL}	R_{UO}	R_M	$\frac{da}{dN}\Big\vert_{SS}^{PRE.\ O.L.}$ (in/cycle)	$\frac{da}{dN}\Big\vert_{SS}^{POST\ O.L.}$ (in/cycle)	$\frac{da}{dN}\Big\vert_{MIN}$ (in/cycle)	N_D (cycles)	Δa* (in)	a_{OL} (in)	Spec.
1	33.33	11.67	0.65	1.00	0.11	0.65	2.58×10^{-5}	2.60×10^{-5}	2.60×10^{-5}	0	0	0.67	A-1
2	25.64	11.50	0.55	1.30	0.11	0.42	2.04×10^{-5}	2.12×10^{-5}	3.65×10^{-6}	6,800	0.061	0.94	A-1
3	20.83	11.50	0.45	1.60	0.11	0.28	1.39×10^{-5}	1.41×10^{-5}	7.76×10^{-7}	22,000	0.079	1.23	A-1
4	17.54	11.50	0.34	1.90	0.11	0.18	1.19×10^{-5}	1.00×10^{-5}	1.86×10^{-7}	121,000	0.138	0.81	A-2
5†	15.15	11.50	0.24	2.20	0.11	0.11	6.53×10^{-6}	-	-	-	-	1.23	A-2
6	20.83	13.50	0.35	1.60	-1.00	0.22	4.04×10^{-5}	3.55×10^{-5}	9.65×10^{-6}	5,850	0.080	1.57	A-5
7	20.83	13.50	0.35	1.60	-0.50	0.22	2.48×10^{-5}	2.66×10^{-5}	5.02×10^{-6}	10,600	0.103	1.46	A-3
8	20.83	13.50	0.35	1.60	0.01	0.22	2.29×10^{-5}	1.78×10^{-5}	2.93×10^{-6}	11,400	0.074	0.84	A-3
9	20.83	13.50	0.35	1.60	0.11	0.22	1.79×10^{-5}	2.00×10^{-5}	2.12×10^{-6}	18,400	0.093	0.49	A-3
10	20.83	13.50	0.35	1.60	0.22	0.22	1.88×10^{-5}	1.78×10^{-5}	5.29×10^{-7}	44,000	0.093	0.52	A-10
11	18.52	11.19	0.40	1.80	-1.00	0.22	1.39×10^{-5}	1.58×10^{-5}	4.31×10^{-6}	11,800	0.074	1.07	A-5
12	18.52	11.19	0.40	1.80	-0.50	0.22	1.94×10^{-5}	1.41×10^{-5}	4.01×10^{-6}	14,400	0.093	0.70	A-5
13	18.52	11.19	0.40	1.80	0.01	0.22	1.24×10^{-5}	1.00×10^{-5}	9.34×10^{-7}	42,600	0.127	0.43	A-6
14	18.52	11.19	0.40	1.80	0.11	0.22	1.16×10^{-5}	1.00×10^{-5}	2.55×10^{-7}	53,000	0.102	1.17	A-4
15	18.52	11.19	0.40	1.80	0.22	0.22	1.12×10^{-5}	1.20×10^{-5}	1.07×10^{-7}	142,000	0.120	0.81	A-6
16	15.15	7.82	0.48	2.20	-1.00	0.22	4.76×10^{-6}	5.01×10^{-6}	1.05×10^{-6}	52,000	0.110	1.27	A-6
17	15.15	7.82	0.48	2.20	-0.50	0.22	6.55×10^{-6}	7.94×10^{-6}	1.92×10^{-7}	127,000	0.170	1.40	A-10
18†	15.15	7.82	0.48	2.20	0.01	0.22	4.88×10^{-6}	-	-	-	-	1.45	A-8
19†	15.15	7.82	0.48	2.20	0.11	0.22	5.93×10^{-6}	-	-	-	-	0.67	A-13
20†	15.15	7.82	0.48	2.20	0.22	0.22	4.81×10^{-6}	-	-	-	-	1.64	A-6
21	18.52	14.85	0.20	1.80	-1.00	0.11	2.18×10^{-5}	1.78×10^{-5}	5.36×10^{-6}	10,300	0.078	1.11	A-13
22	18.52	14.85	0.20	1.80	-0.05	0.11	3.10×10^{-5}	1.41×10^{-5}	4.41×10^{-6}	17,600	0.125	0.41	A-9
23	18.52	14.85	0.20	1.80	0.01	0.11	2.32×10^{-5}	1.78×10^{-5}	3.29×10^{-7}	44,500	0.068	1.70	A-8
24	18.52	14.85	0.20	1.80	0.11	0.11	2.02×10^{-5}	2.00×10^{-5}	3.54×10^{-7}	63,700	0.137	0.43	A-7
*													
30	18.52	8.52	0.54	1.80	-1.00	0.30	7.59×10^{-6}	7.24×10^{-6}	1.06×10^{-6}	25,000	0.093	2.03	A-6
31	18.52	8.52	0.54	1.80	-0.50	0.30	9.61×10^{-6}	7.94×10^{-6}	2.39×10^{-6}	17,600	0.065	0.97	A-10
32	18.52	8.52	0.54	1.80	0.01	0.30	6.67×10^{-6}	6.31×10^{-6}	5.90×10^{-7}	52,800	0.059	0.47	A-8
33	18.52	8.52	0.54	1.80	0.11	0.30	6.31×10^{-6}	6.33×10^{-6}	2.81×10^{-7}	83,200	0.118	0.74	A-8
34	18.52	8.52	0.54	1.80	0.22	0.30	6.33×10^{-6}	7.08×10^{-6}	1.03×10^{-7}	197,000	0.123	0.98	A-8
35	18.52	8.52	0.54	1.80	0.30	0.30	7.08×10^{-6}	-	-	-	-	1.21	A-8
16-2.4†	13.89	6.56	0.53	2.40	-1.00	0.22	3.88×10^{-6}	2.82×10^{-6}	3.14×10^{-7}	124,000	0.113	1.64	A-13
16-2.6	12.82	5.49	0.57	2.60	-1.00	0.22	1.52×10^{-6}	2.63×10^{-6}	1.27×10^{-7}	260,000	0.115	1.09	A-14
17-2.4	13.89	6.56	0.53	2.40	-0.50	0.22	3.57×10^{-6}	2.14×10^{-6}	5.55×10^{-7}	126,000	0.137	0.45	A-14
3A/D-.4a†	11.11	7.78	0.30	3.00	-0.40	0.10	5.15×10^{-6}	-	-	-	-	1.56	A-14
3A/D-.4b†	11.11	7.78	0.30	3.00	-0.40	0.10	4.00×10^{-6}	-	-	-	-	0.72	A-15
3A/D-.5	11.11	7.78	0.30	3.00	-0.50	0.10	4.93×10^{-6}	2.82×10^{-6}	1.05×10^{-7}	593,000	0.150	0.48	A-15
R-12	18.52	11.19	0.40	1.80	-0.50	0.22	4.02×10^{-5}	1.00×10^{-5}	7.72×10^{-8}	160,550	0.089	0.52	A-12
R-13	18.52	11.19	0.40	1.80	0.01	0.22	1.05×10^{-5}	9.33×10^{-6}	1.52×10^{-7}	169,000	0.100	0.48	A-11

* Tests 25-29 are the same as Tests 11-15

† Tests arrested - $N_D > 10^6$ cycles; $\frac{da}{dN}\Big\vert_{MIN} < 4\times10^{-10}$ in/cycles

NOTE: K_{OL} = 33.33 ksi$\sqrt{in}$ for all Tests.

$2r_y$ = 0.109 in for all Tests.

Overload Preceeded Underload Except in Tests R-12, R-13.

TABLE II

RESIDUAL STRESS INTENSITY PARAMETERS

Test No.	Q_{OL}	R_{UO}	R_M	R_{EFF}^{MIN}	K_R^{MAX}
1	1.00	0.11	0.65	+0.65	0
2	1.30	0.11	0.42	-0.13	12.31
3	1.60	0.11	0.28	-1.18	15.54
4	1.90	0.11	0.18	-1.40	12.73
5	2.20	0.11	0.11	-	-
6	1.60	-1.00	0.22	+0.10	5.80
7	1.60	-0.50	0.22	-0.26	10.09
8	1.60	0.01	0.22	-0.56	12.15
9	1.60	0.11	0.22	-0.71	12.95
10	1.60	0.22	0.22	-1.25	14.84
11	1.80	-1.00	0.22	+0.05	6.80
12	1.80	-0.50	0.22	+0.02	7.16
13	1.80	0.01	0.22	-0.78	12.24
14	1.80	0.11	0.22	-1.27	13.59
15	1.80	0.22	0.22	-1.51	14.07
16	2.20	-1.00	0.22	+0.01	7.24
17	2.20	-0.50	0.22	-0.91	11.06
18	2.20	0.01	0.22	-	-
19	2.20	0.11	0.22	-	-
20	2.20	0.22	0.22	-	-
21	1.80	-1.00	0.11	-0.42	8.03
22	1.80	-0.50	0.11	-0.52	8.75
23	1.80	0.01	0.11	-1.49	12.54
24	1.80	0.11	0.11	-1.47	12.50
*					
30	1.80	-1.00	0.30	-0.20	11.43
31	1.80	-0.50	0.30	+0.21	7.68
32	1.80	0.01	0.30	-0.53	12.97
33	1.80	0.11	0.30	-0.89	13.99
34	1.80	0.22	0.30	-1.25	14.73
35	1.80	0.30	0.30	-	-
16-2.4	2.40	-1.00	0.22	-0.37	9.09
16-2.6	2.60	-1.00	0.22	-0.51	9.19
17-2.4	2.40	-0.50	0.22	-0.02	7.45
3A/D-.4a	3.00	-0.40	0.10	-	-
3A/D-.4b	3.00	-0.40	0.10	-	-
3A/D-.5	3.00	-0.50	0.10	-1.14	7.47

* Tests 25-29 are the same as Tests 11-15.

TABLE III

PREDICTED AND EXPERIMENTAL RESULTS FROM EXTENDED CRACK CLOSURE CONCEPTS

Test No.	Q_{OL}	R_{UO}	R_M	K_{OP}^{MAX} EXPERIMENT (ksi$\sqrt{in}$)	K_{OP}^{MAX} PREDICTED (ksi$\sqrt{in}$)	$\frac{da}{dN}\vert_{MIN}$ EXPERIMENT (in/cycle)	$\frac{da}{dN}\vert_{MIN}$ PREDICTED (in/cycle)	N_D EXPERIMENT cycles	N_D PREDICTED cycles
1	1.00	0.11	0.65	24.89	17.76	2.60×10^{-5}	2.77×10^{-4}	0	580
2	1.30	0.11	0.42	20.57	17.10	3.65×10^{-6}	2.73×10^{-5}	6,800	3,150
3	1.60	0.11	0.28	18.01	16.43	3.79×10^{-7}	2.11×10^{-6}	22,000	20,450
4	1.90	0.11	0.18	15.20	15.76	1.86×10^{-7}	6.42×10^{-8}	121,000	262,300
5†	2.20	0.11	0.11	≥15.15	15.09	-	1.08×10^{-13}	-	$>10^6$
6	1.60	-1.00	0.22	14.31	14.80	9.65×10^{-6}	7.13×10^{-6}	5,850	8,400
7	1.60	-0.50	0.22	15.32	14.60	5.02×10^{-6}	7.86×10^{-6}	10,600	7,800
8	1.60	0.01	0.22	16.04	15.79	2.93×10^{-6}	3.57×10^{-6}	11,400	13,900
9	1.60	0.11	0.22	16.42	16.43	2.12×10^{-6}	2.11×10^{-6}	18,400	20,500
10	1.60	0.22	0.22	17.76	17.36	5.29×10^{-7}	8.47×10^{-7}	44,000	34,900
11	1.80	-1.00	0.22	13.22	13.80	4.31×10^{-6}	2.76×10^{-6}	11,800	16,800
12	1.80	-0.50	0.22	13.32	13.89	4.01×10^{-6}	2.55×10^{-6}	14,400	17,800
13	1.80	0.01	0.22	14.96	15.29	9.34×10^{-7}	6.36×10^{-7}	42,600	49,200
14	1.80	0.11	0.22	15.98	15.98	2.55×10^{-7}	2.50×10^{-7}	53,000	97,200
15	1.80	0.22	0.22	16.49	16.97	1.07×10^{-7}	3.75×10^{-8}	142,000	388,800
16	2.20	-1.00	0.22	11.48	11.80	1.05×10^{-6}	7.37×10^{-7}	52,000	44,200
17	2.20	-0.50	0.22	12.79	12.39	1.92×10^{-7}	3.46×10^{-7}	127,000	76,700
18†	2.20	0.01	0.22	≥15.15	14.30	-	3.67×10^{-9}	-	$>10^6$
19†	2.20	0.11	0.22	≥15.15	15.09	-	1.08×10^{-13}	-	$>10^6$
20†	2.20	0.22	0.22	≥15.15	16.19	-	-	-	$>10^6$
21	1.80	-1.00	0.11	12.92	13.80	5.36×10^{-6}	2.76×10^{-6}	10,300	16,800
22	1.80	-0.50	0.11	13.20	13.89	4.41×10^{-6}	2.55×10^{-6}	17,600	17,800
23	1.80	0.01	0.11	15.80	15.29	3.29×10^{-7}	6.36×10^{-7}	44,500	49,200
24	1.80	0.11	0.11	15.75	15.98	3.54×10^{-7}	2.50×10^{-7}	63,700	97,200
*									
30	1.80	-1.00	0.30	14.84	13.80	1.06×10^{-6}	2.76×10^{-6}	25,000	16,800
31	1.80	-0.50	0.30	13.98	13.89	2.39×10^{-6}	2.55×10^{-6}	17,600	17,800
32	1.80	0.01	0.30	15.36	15.29	5.90×10^{-7}	6.36×10^{-7}	52,800	49,200
33	1.80	0.11	0.30	15.90	15.98	2.81×10^{-7}	2.50×10^{-7}	83,200	97,200
34	1.80	0.22	0.30	16.51	16.97	1.03×10^{-7}	3.75×10^{-8}	197,000	388,800
35†	1.80	0.30	0.30	≥18.52	17.85	-	1.47×10^{-9}	-	$>10^6$
16-2.4	2.40	-1.00	0.22	11.21	10.80	3.14×10^{-7}	5.38×10^{-7}	124,000	55,600
16-2.6	2.60	-1.00	0.22	10.69	9.80	1.27×10^{-7}	4.93×10^{-7}	260,000	59,200
17-2.4	2.40	-0.50	0.22	10.77	11.64	5.55×10^{-7}	1.56×10^{-7}	126,000	137,000
3A/D-.4a†	3.00	-0.40	0.10	≥11.11	9.77	-	2.15×10^{-8}	-	584,900
3A/D-.4b†	3.00	-0.40	0.10	≥11.11	9.77	-	2.15×10^{-8}	-	584,900
3A/D-.5	3.00	-0.50	0.10	9.09	9.39	1.05×10^{-7}	5.55×10^{-8}	593,000	292,000

* Tests 25-29 are the same as Tests 11-15.

† Tests arrested - $N_D > 10^6$ cycles ; $\frac{da}{dN}\vert_{MIN} < 4\times10^{-10}$ in/cycle

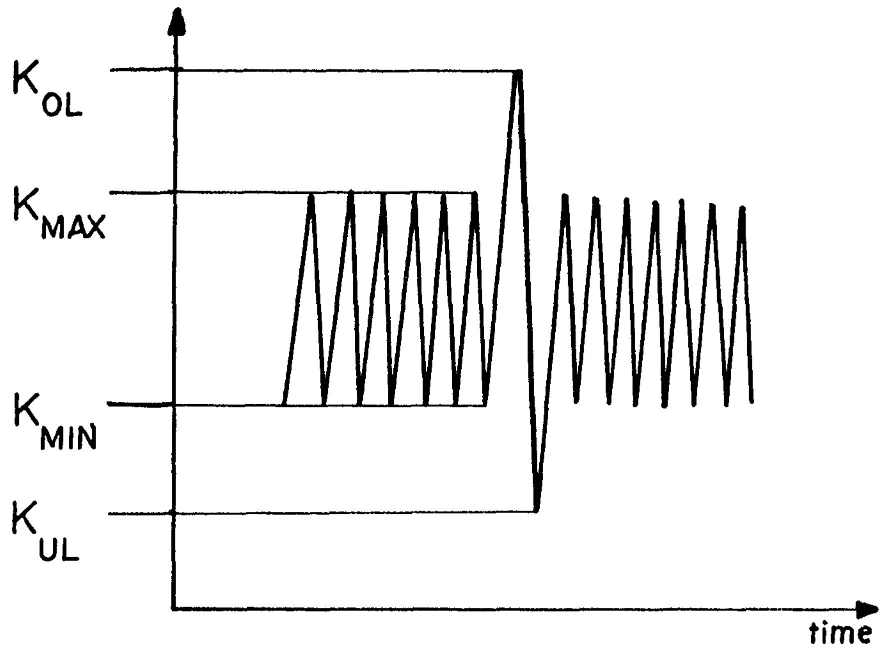

$$R_{UO} = \frac{K_{UL}}{K_{OL}} \qquad R_M = \frac{K_{MIN}}{K_{OL}}$$

$$R_F = \frac{K_{MIN}}{K_{MAX}} \qquad Q_{OL} = \frac{K_{OL}}{K_{MAX}}$$

Figure 1. Definition of variables

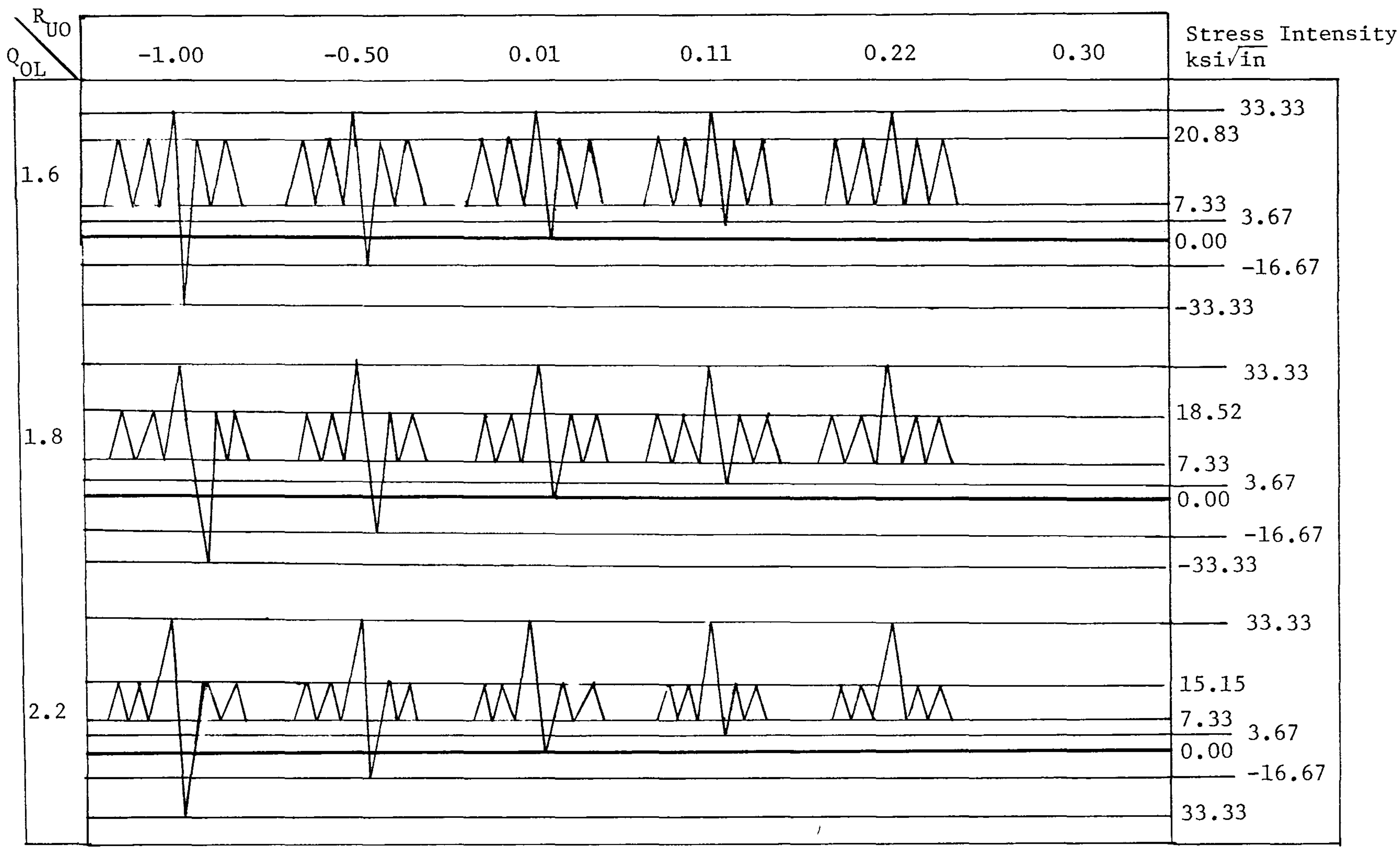

$R_M = 0.22$, K_{MIN} constant

Figure 2. Q_{OL} vs. R_{UO} test matrix

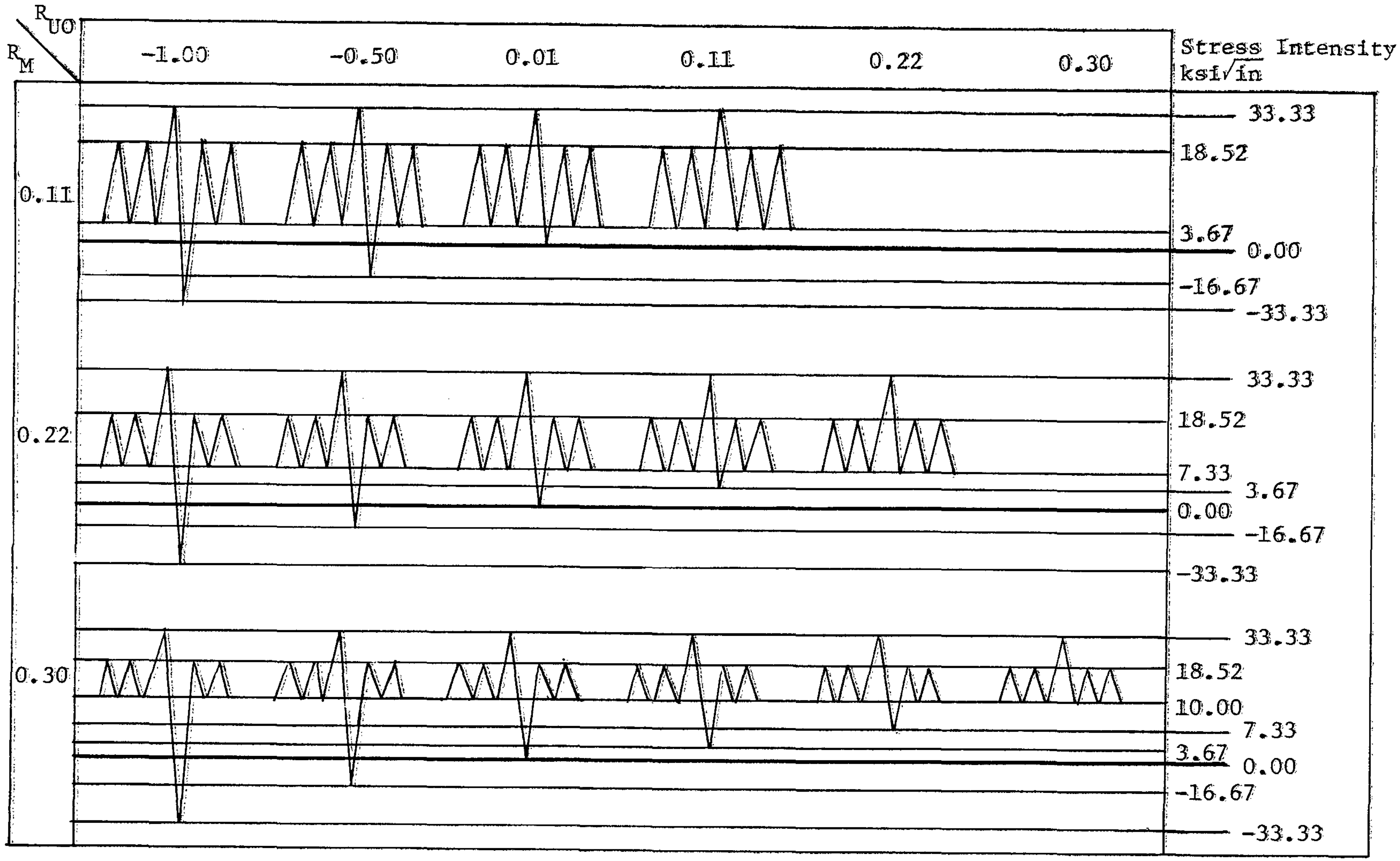

$Q_{OL} = 1.8$, K_{MAX} constant

Figure 3. R_M vs. R_{UO} test matrix

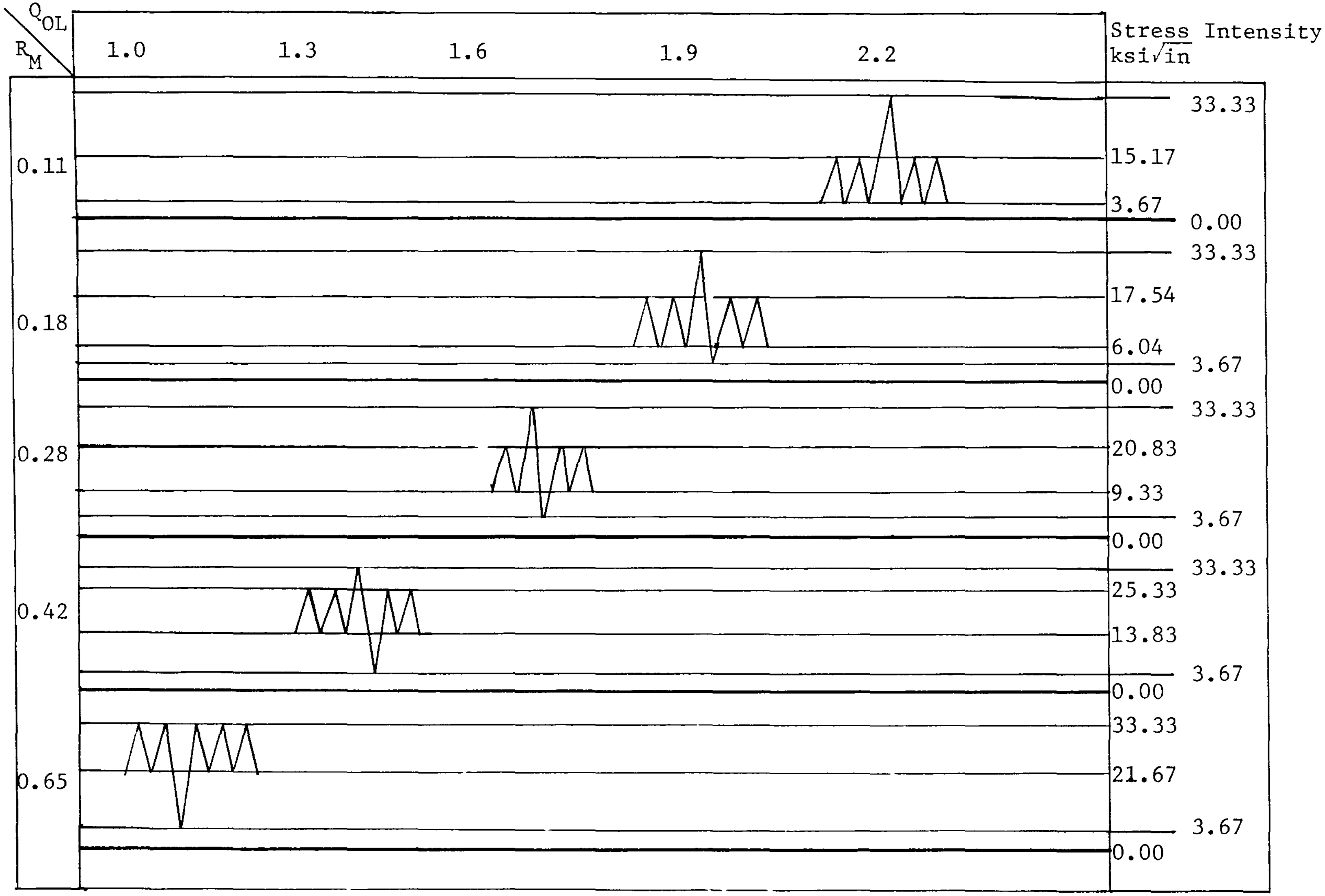

$R_{UO} = 0.11$, K_{UL} constant

Figure 4. R_M vs. Q_{OL} test matrix

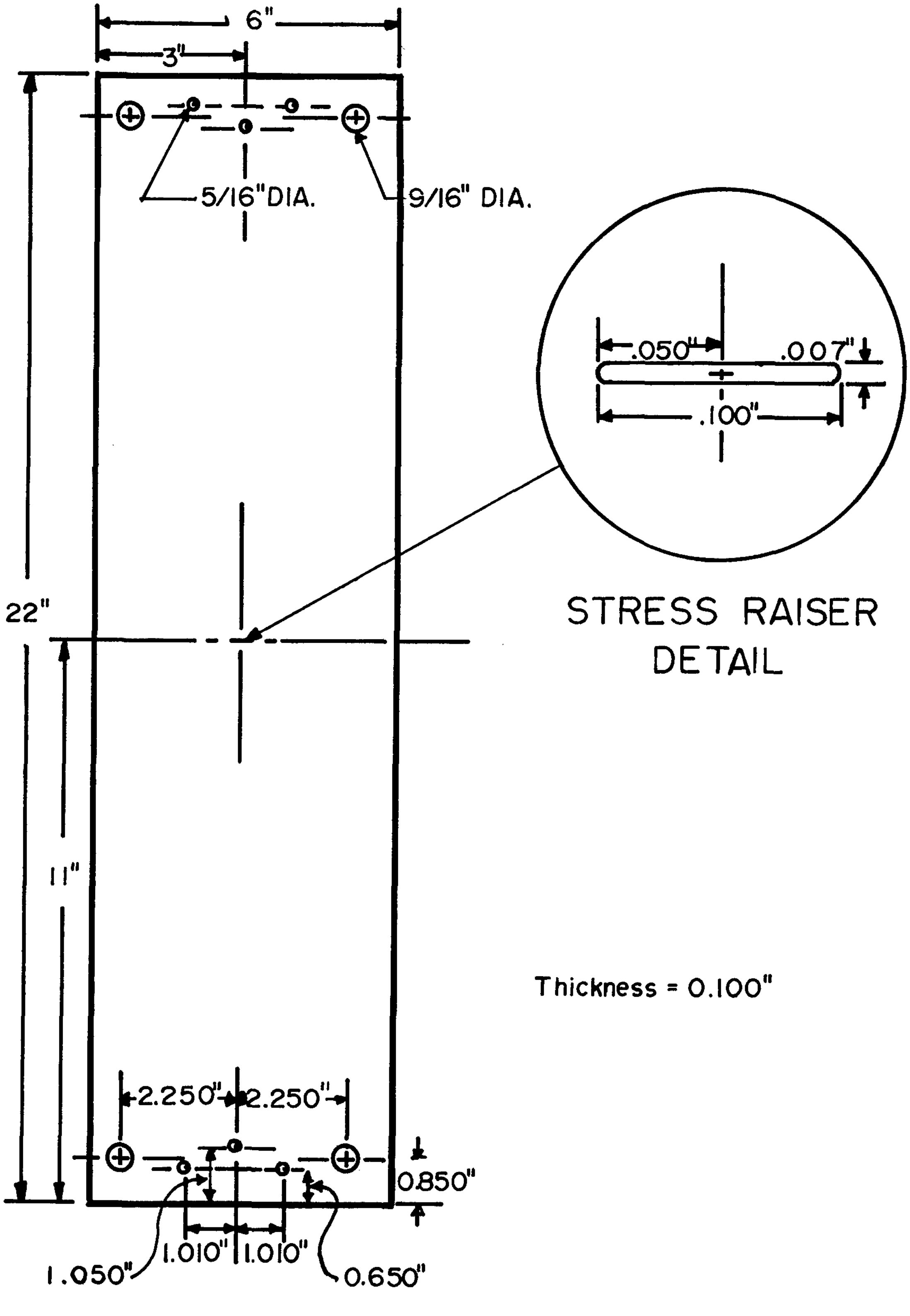

Figure 5. Center crack test specimen

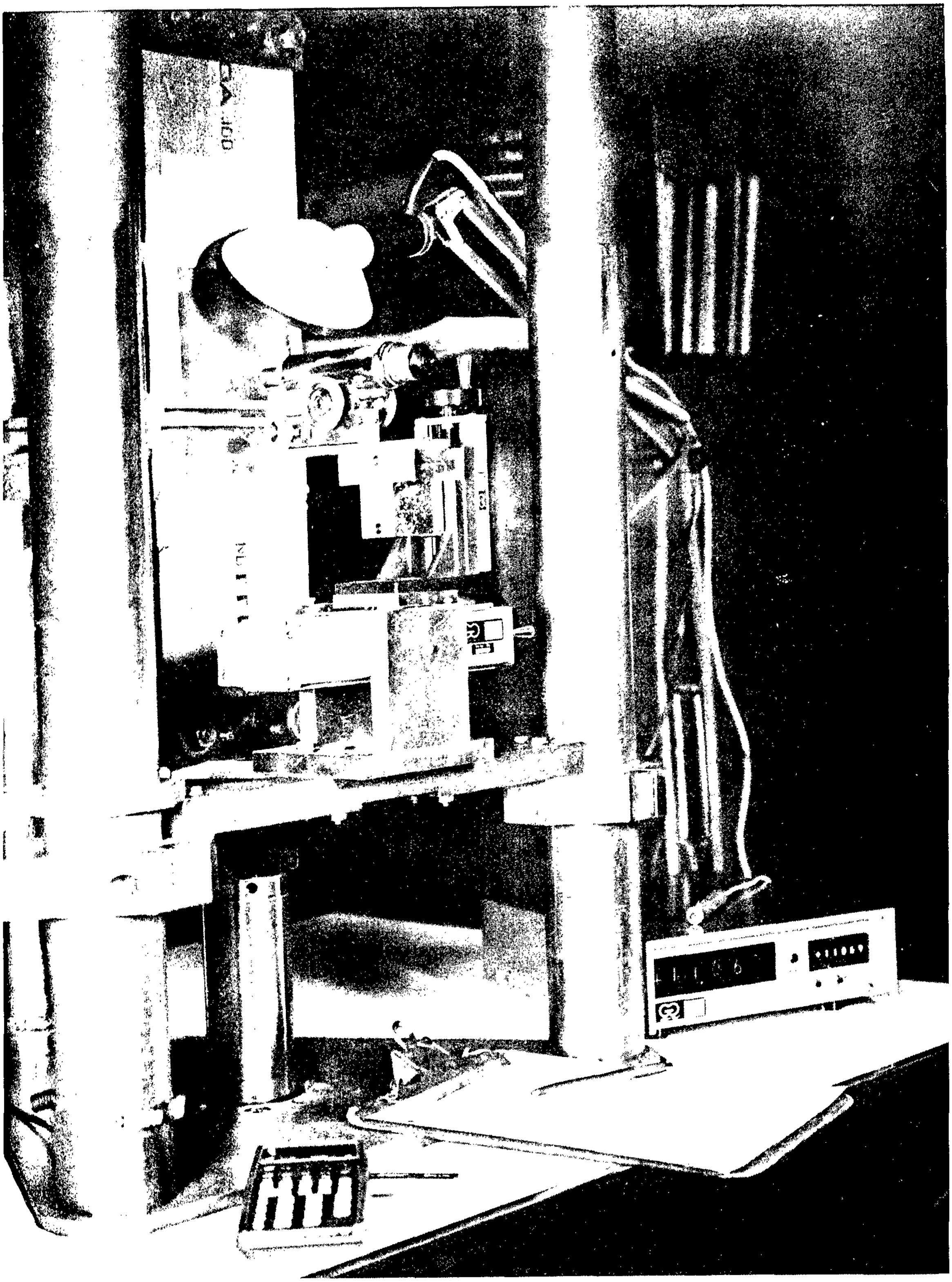

Figure 6. Microscope and traverse system

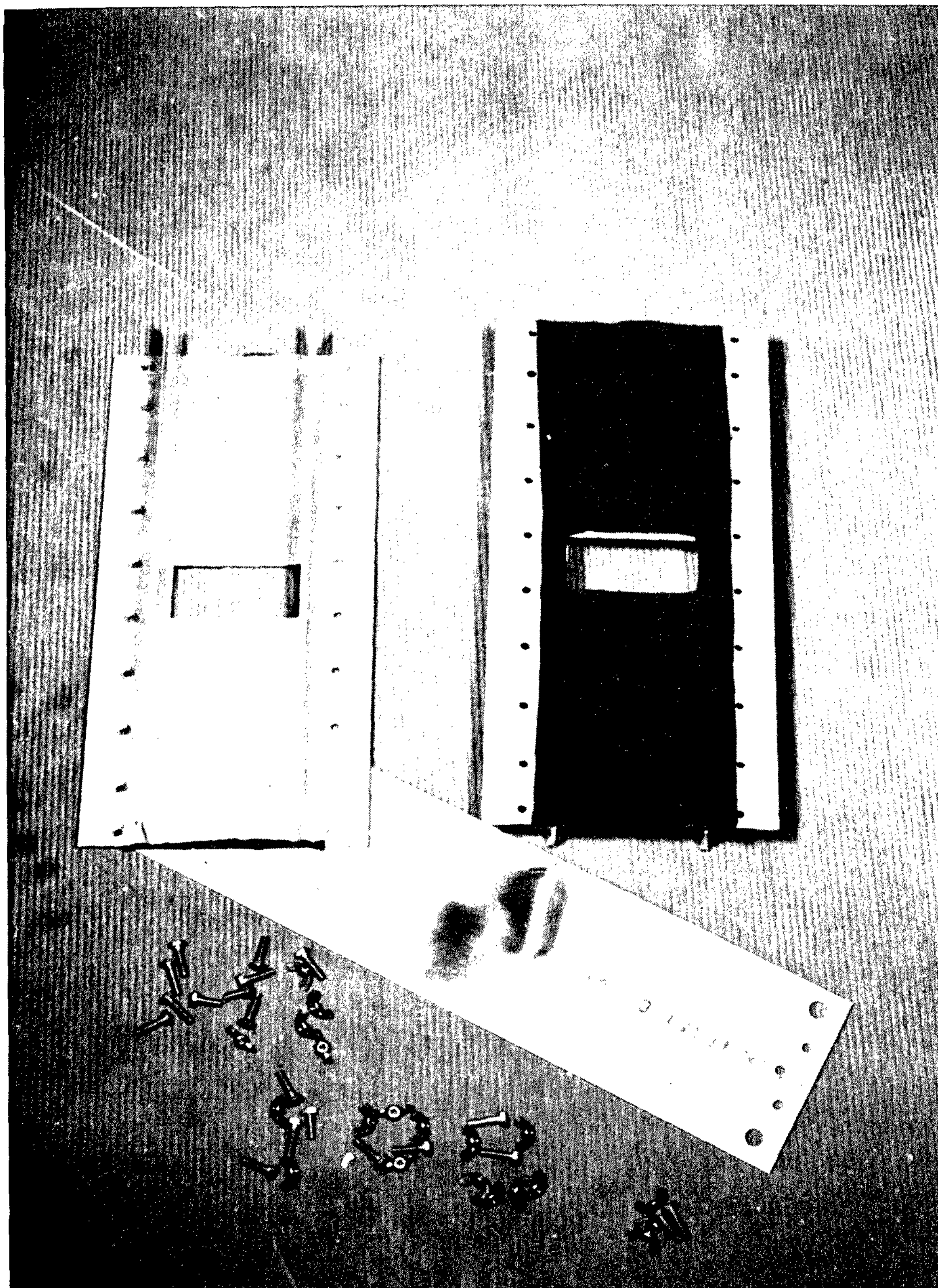

Figure 7. Compression guides and specimen

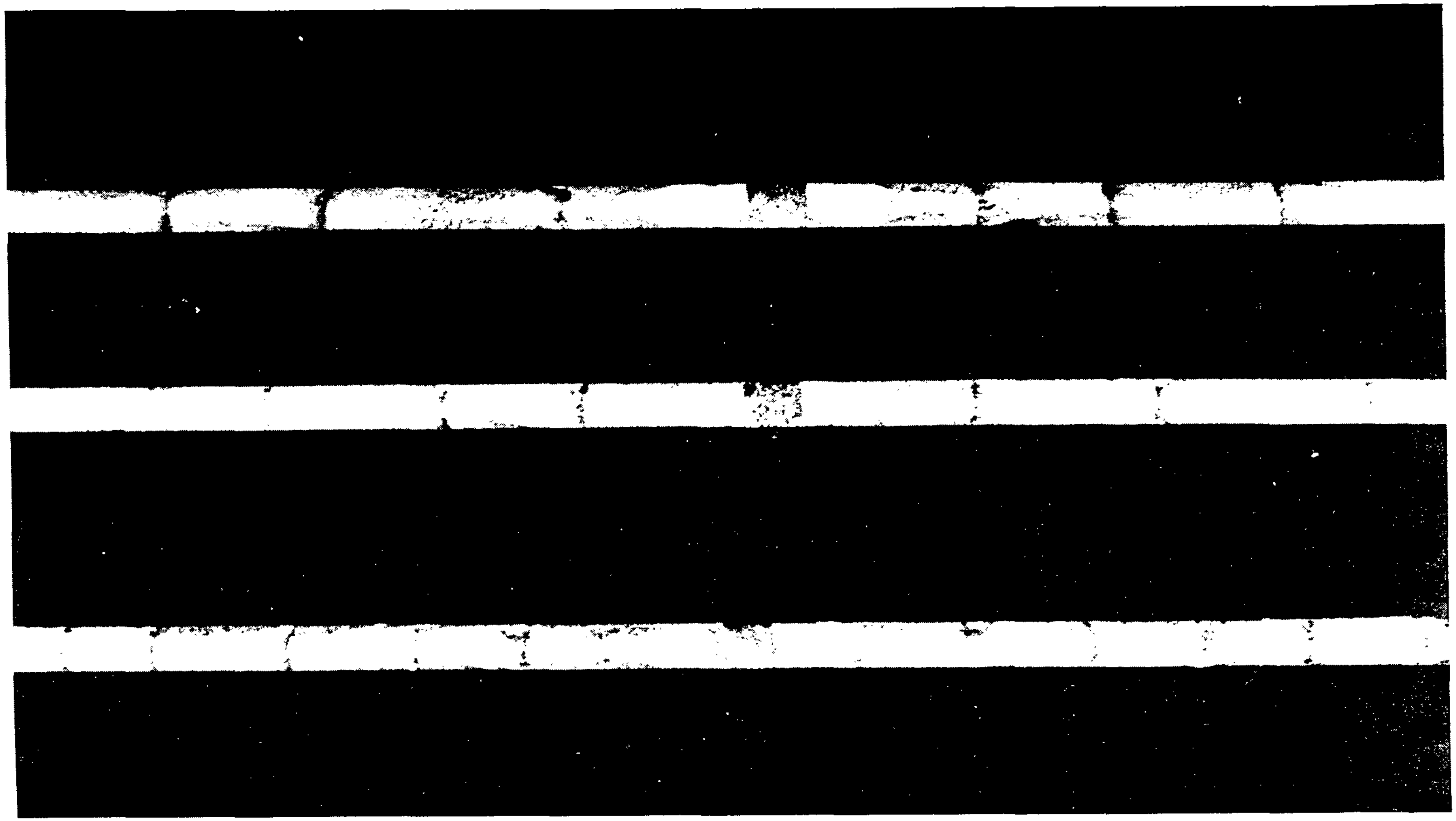

Figure 8. Typical fracture surfaces for specimens A-5, A-6 and A-8.

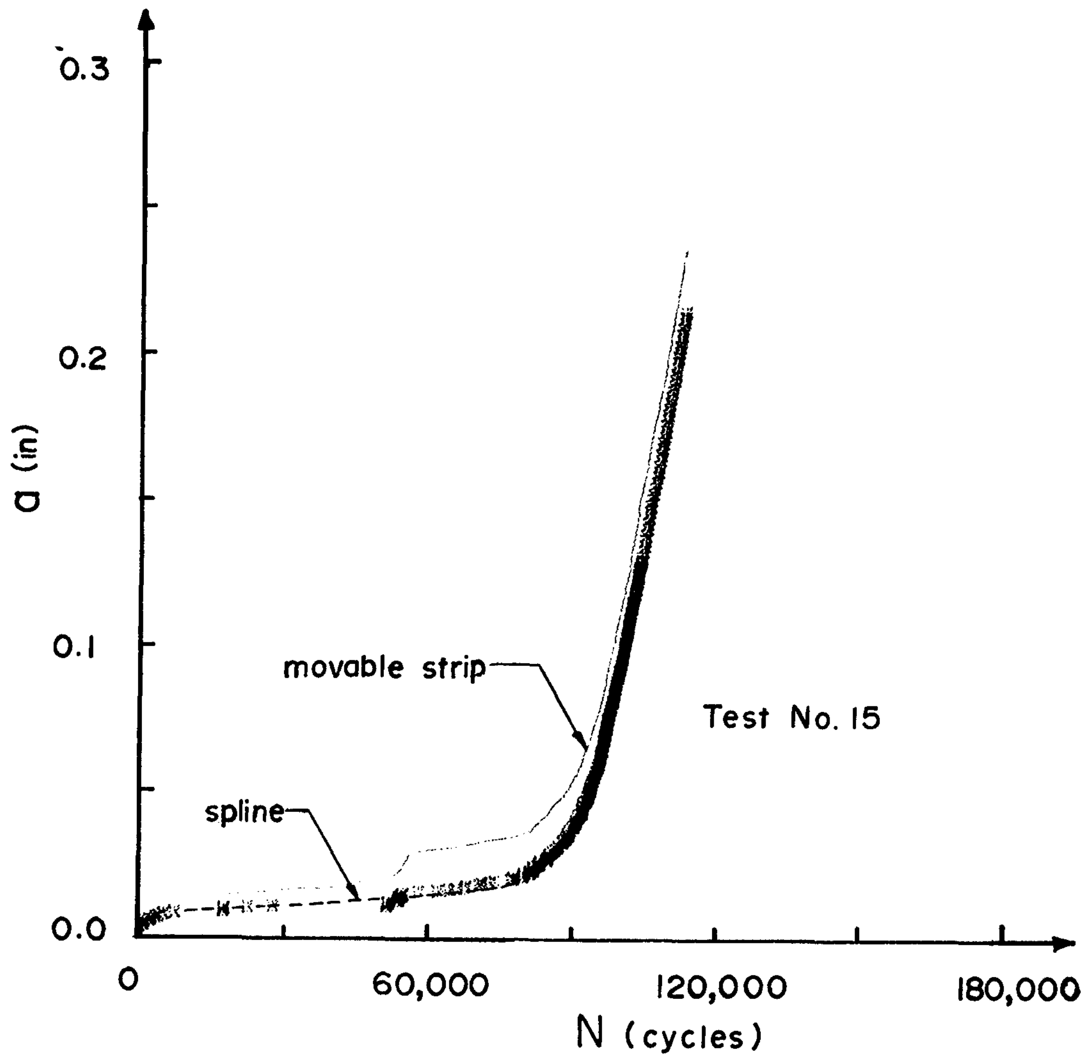

Figure 9. Spline function and integrated $\frac{da}{dN}$ from the movable strip method for a versus N data

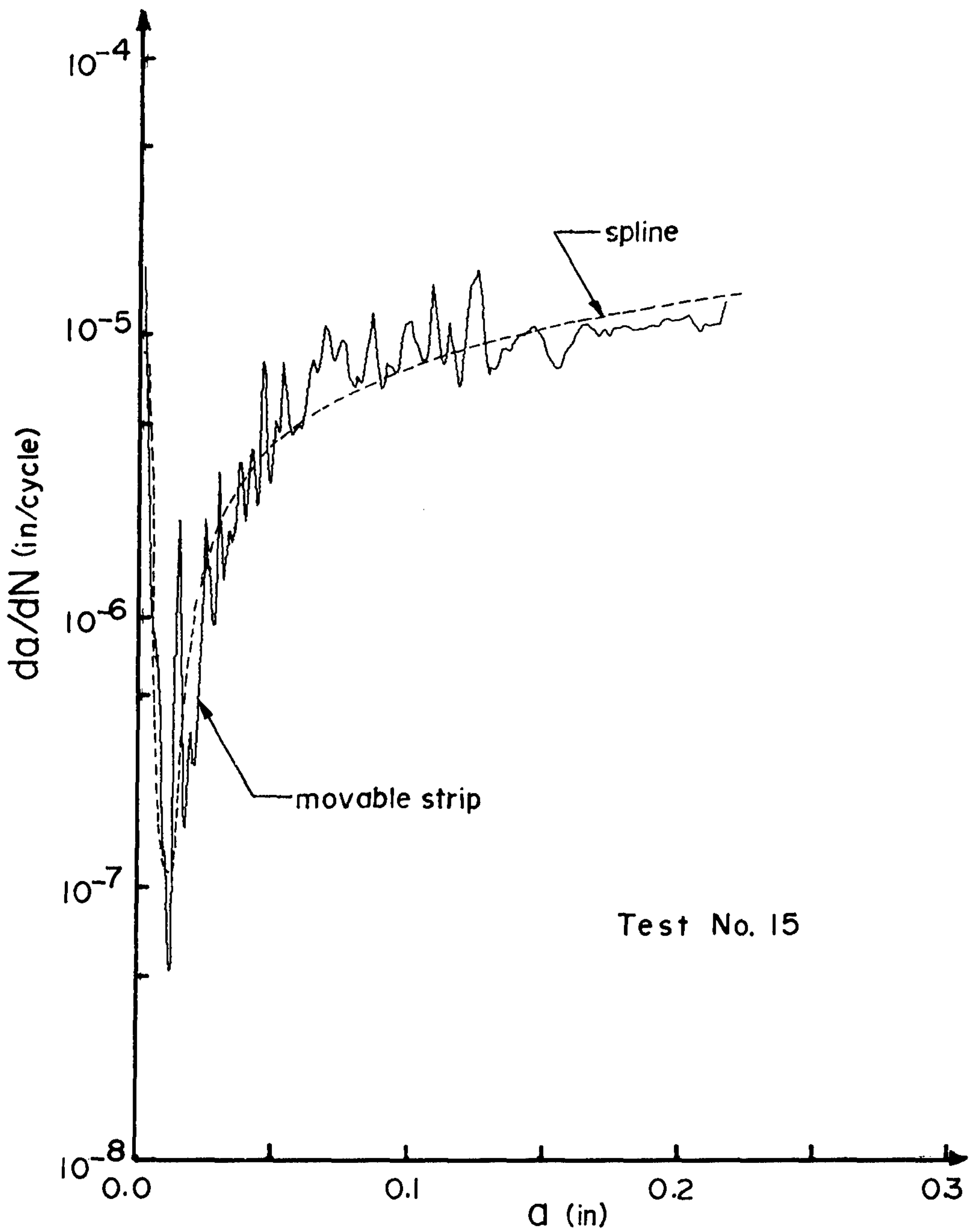

Figure 10. Comparison of da/dN obtained from the spline function and from the movable strip method

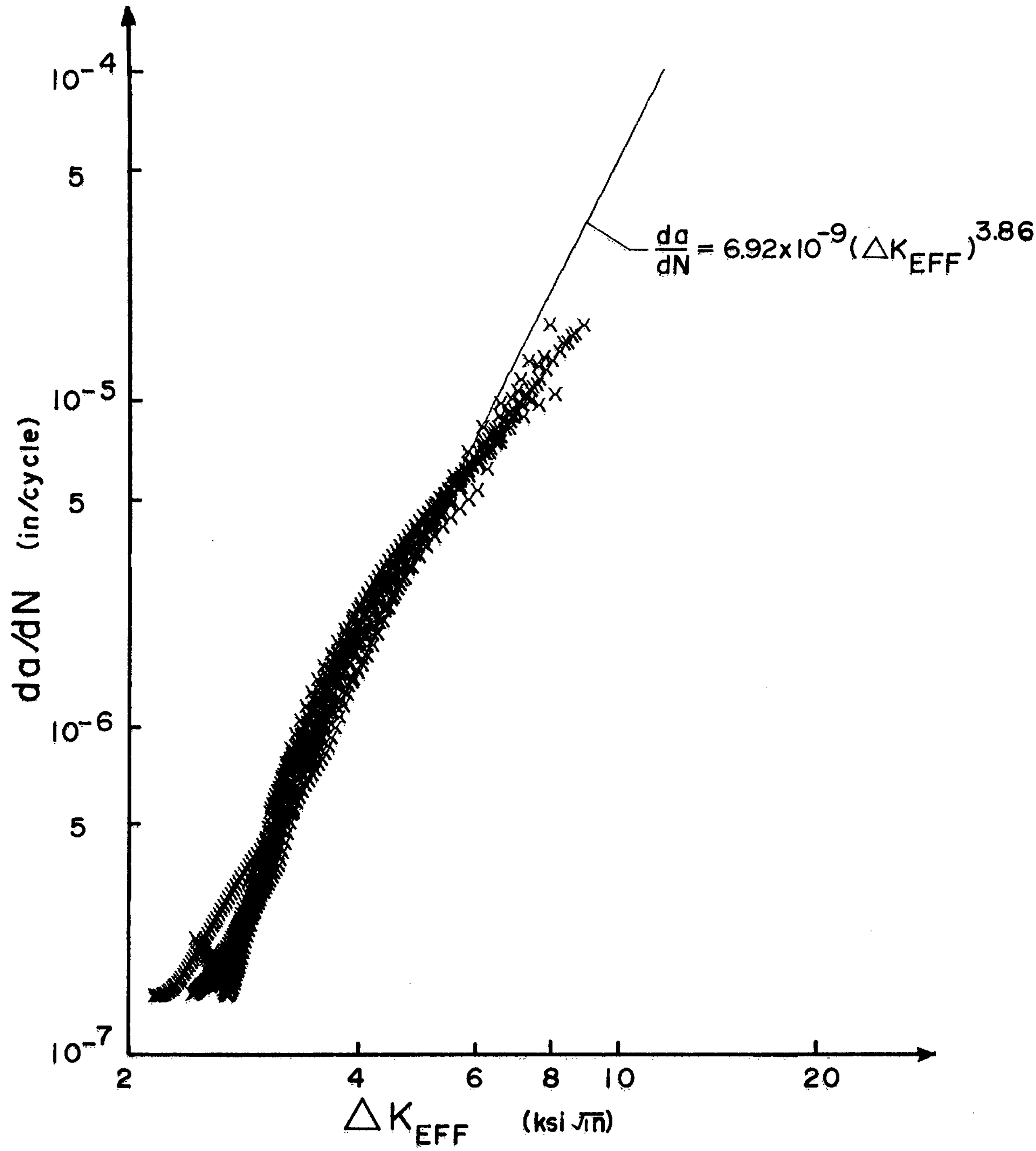

Figure 11. Constant stress amplitude data (showing alternate points only) and least square fit line for Equation 4 where $\Delta K_{EFF} = 0.5 + 0.4R_F$

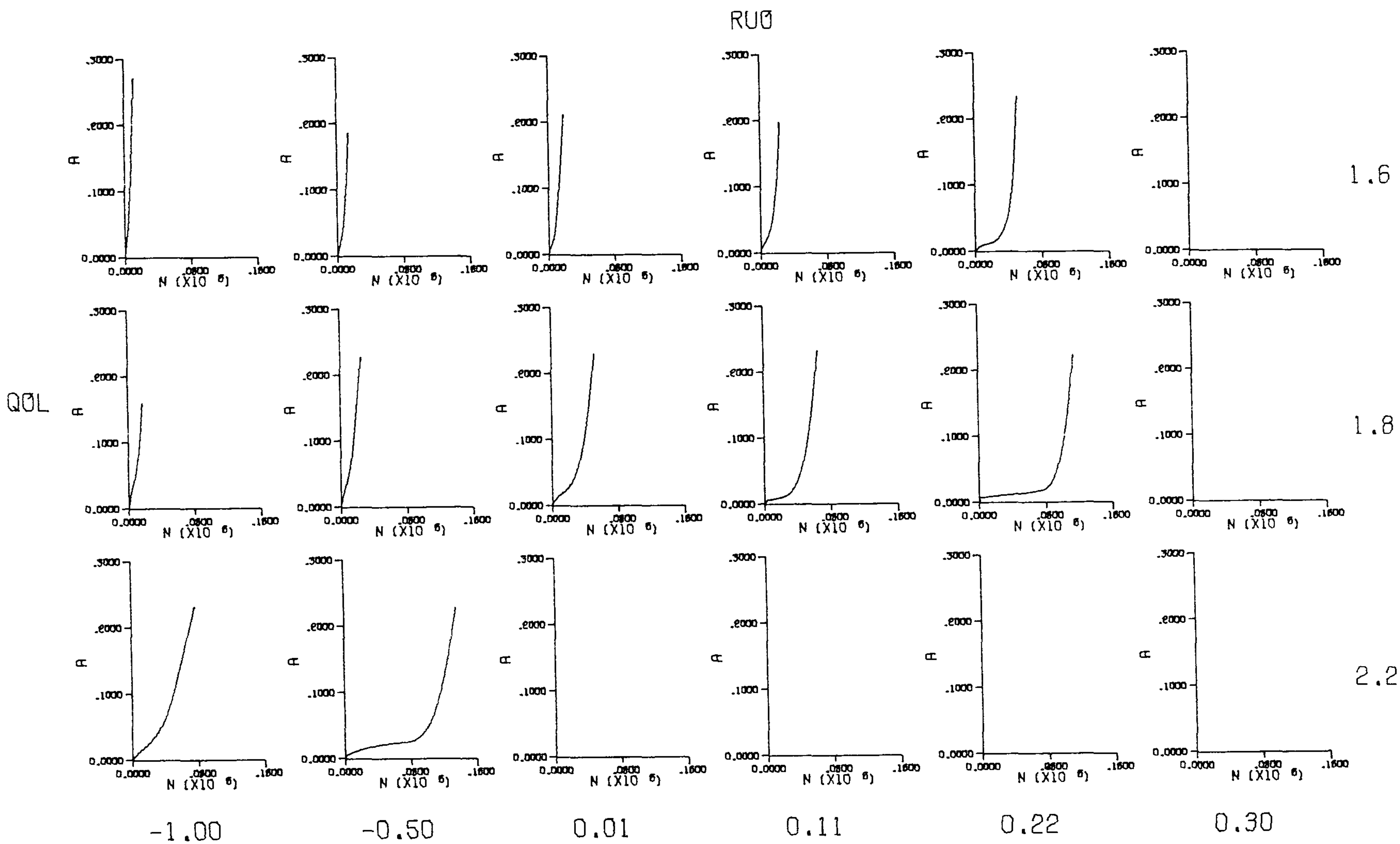

Figure 12. a vs. N curves for test in the Q_{OL} vs. R_{UO} plane (K_{MIN} = 7.33 ksi$\sqrt{in}$)

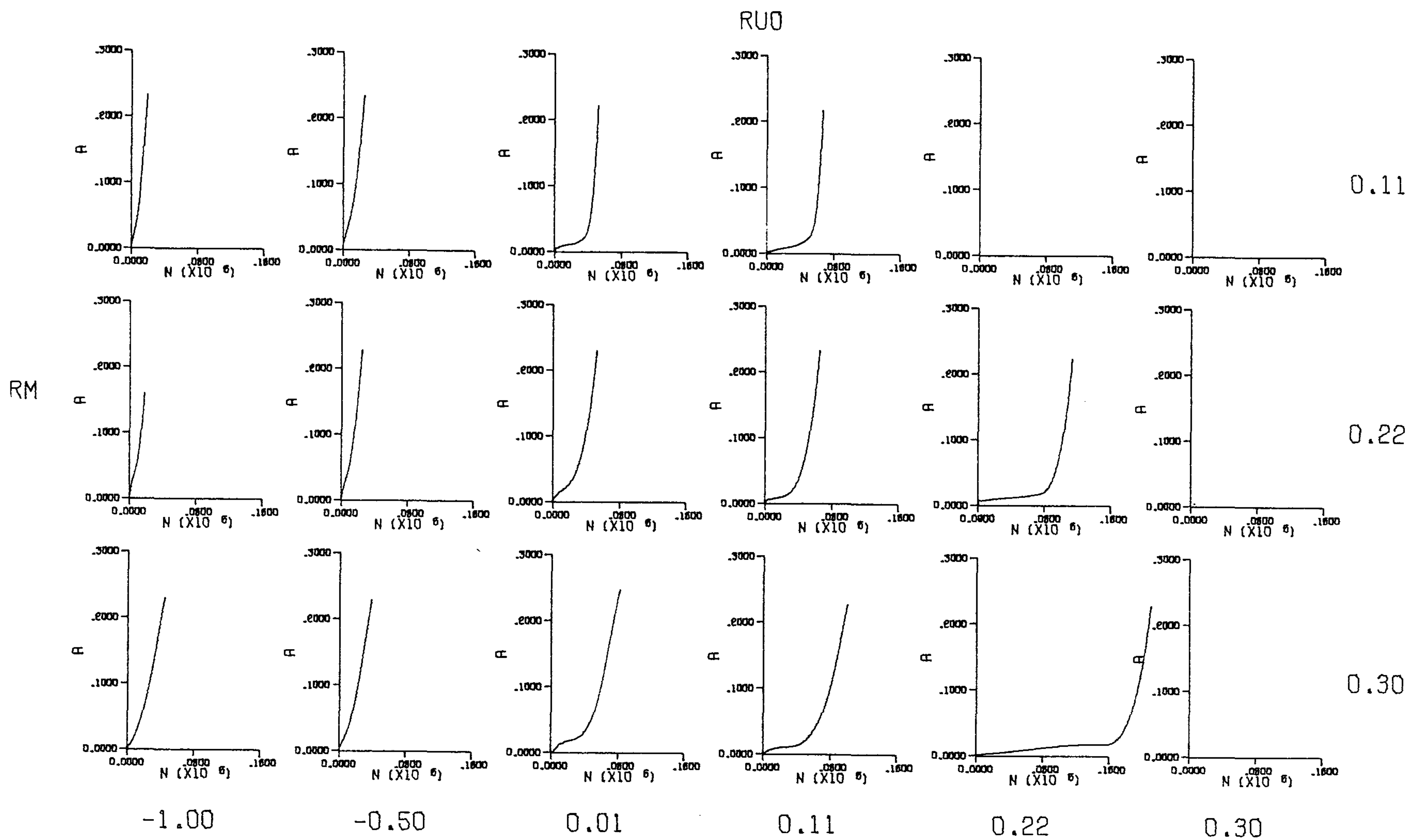

Figure 13. a vs. N curves for tests in the R_M vs. R_{UO} plane (K_{MAX} = 18.52 ksi$\sqrt{in}$)

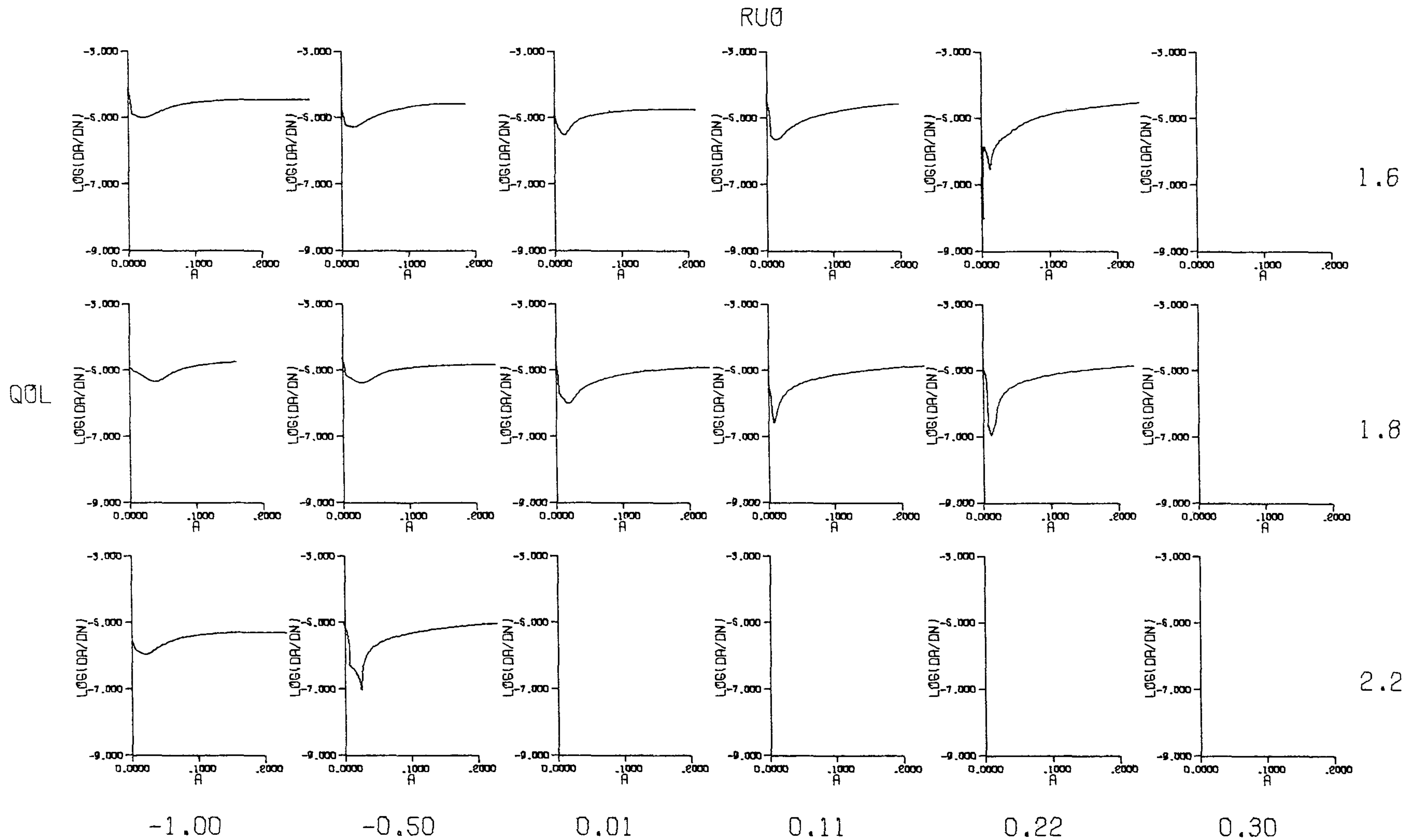

Figure 14. $\frac{da}{dN}$ vs. a for tests in the Q_{OL} vs. R_{UO} plane (K_{MIN} = 7.33 ksi$\sqrt{in}$)

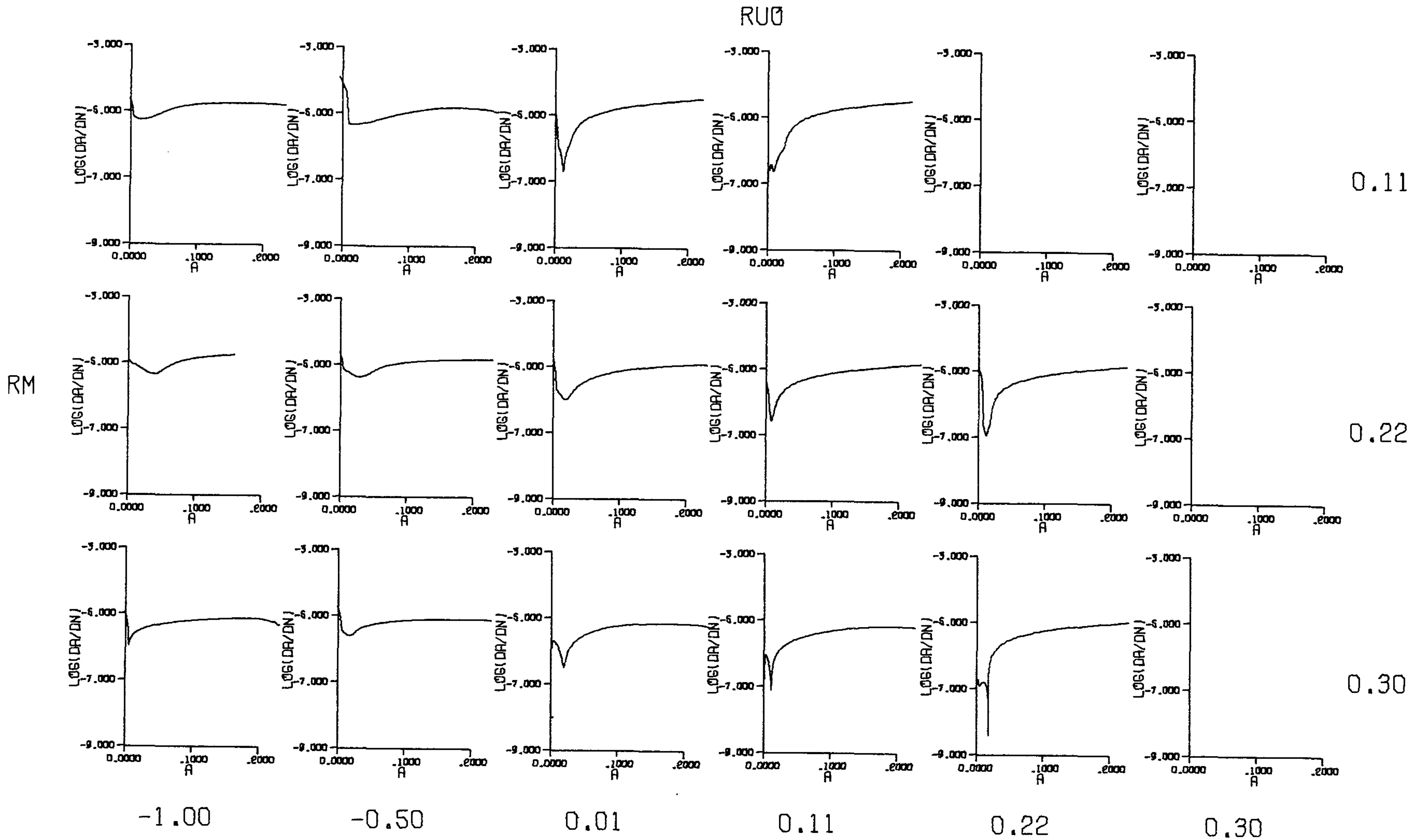

Figure 15. $\frac{da}{dN}$ vs. a for tests in the R_M vs. R_{UO} plane (K_{MAX} = 18.52 ksi$\sqrt{in}$)

Q_{OL} \ R_{UO}		-1.00	-0.50	0.01	0.11	0.22	0.30
1.6	$\frac{da}{dN}\Big\|_{MIN}$	9.65×10^{-6}	5.02×10^{-6}	2.93×10^{-6}	2.12×10^{-6}	5.29×10^{-7}	
	N_D	5,850	10,600	11,400	18,400	44,000	
1.8	$\frac{da}{dN}\Big\|_{MIN}$	4.31×10^{-6}	4.01×10^{-6}	9.34×10^{-7}	2.55×10^{-7}	1.07×10^{-7}	
	N_D	11,800	14,400	42,600	53,000	142,000	
2.2	$\frac{da}{dN}\Big\|_{MIN}$	1.05×10^{-6}	1.92×10^{-7}	0	0	0	
	N_D	52,000	127,000	∞	∞	∞	

$R_M = 0.22 \quad (K_{MIN} = 7.33 \text{ ksi}\sqrt{\text{in}})$

Figure 16. Minimum growth rate, $da/dN|_{MIN}$, and number of delay cycles, N_D for Q_{OL} vs. R_{UO} plane

R_M	R_{UO}	-1.0	-0.5	0.01	0.11	0.22	0.30
0.11	$\frac{da}{dN}\Big\|_{MIN}$	5.36×10^{-6}	4.41×10^{-6}	3.29×10^{-7}	3.54×10^{-7}		
	N_D	10,300	17,600	44,500	63,700		
0.22	$\frac{da}{dN}\Big\|_{MIN}$	4.31×10^{-6}	4.01×10^{-6}	9.34×10^{-7}	2.55×10^{-7}	1.07×10^{-7}	
	N_D	11,800	14,400	42,600	53,000	142,000	
0.30	$\frac{da}{dN}\Big\|_{MIN}$	1.06×10^{-6}	2.39×10^{-6}	5.90×10^{-7}	2.81×10^{-7}	1.03×10^{-7}	0
	N_D	25,000	17,600	52,800	83,200	197,000	∞

$Q_{OL} = 1.8$ ($K_{MAX} = 18.52$ ksi$\sqrt{in}$)

Figure 17. Minimum growth rate, $da/dN|_{MIN}$, and number of delay cycles, N_D, for R_M vs. R_{UO} plane

Q_{OL} \ R_{UO}	-1.00	-.50	0.01	0.11	0.22	0.30
1.6	0.73	0.94	0.68	0.85	0.85	
1.8	0.68	0.85	1.17	0.94	1.10	
2.2	1.01	1.56	*	*	*	

(a) Q_{OL} - R_{UO} plane, R_M = 0.22 (K_{MIN} = 7.33 ksi$\sqrt{in}$)

Q_{OL} \ R_{UO}	-1.00	-.50	0.01	0.11	0.22	0.30
0.11	0.72	1.15	0.62	1.26		
0.22	0.68	0.85	1.17	0.94	1.10	
0.30	0.85	0.60	0.54	1.08	1.13	*

(b) R_M - R_{UO} plane, Q_{OL} = 1.8 (K_{MAX} = 18.52 ksi$\sqrt{in}$)

* crack arrest

Figure 18. Ratio of measured delay zone size to the plane stress plastic zone size, $\Delta a^*/2r_y$

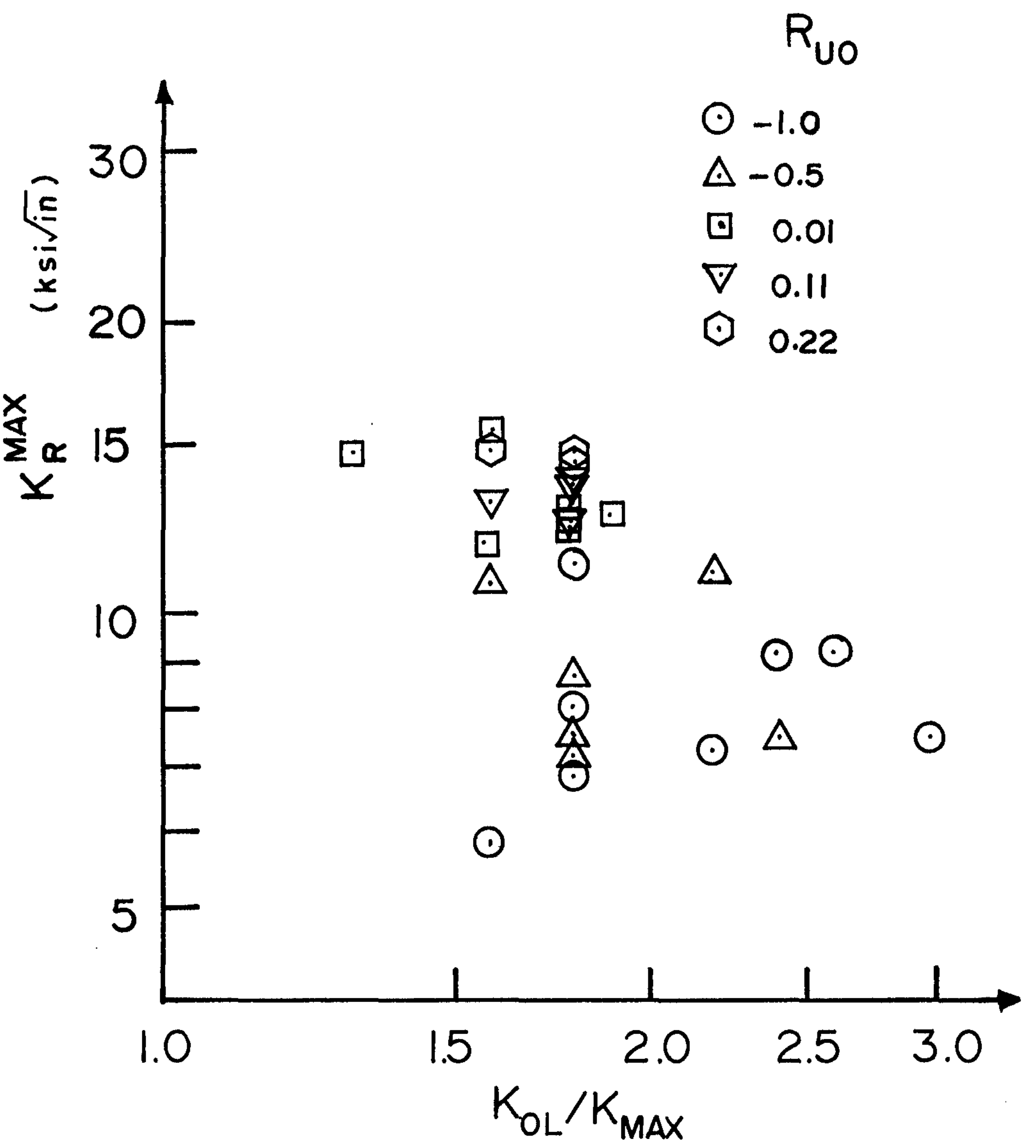

Figure 19. Comparison of maximum residual stress intensity with Wheeler parameter, K_{OL}/K_{MAX}.

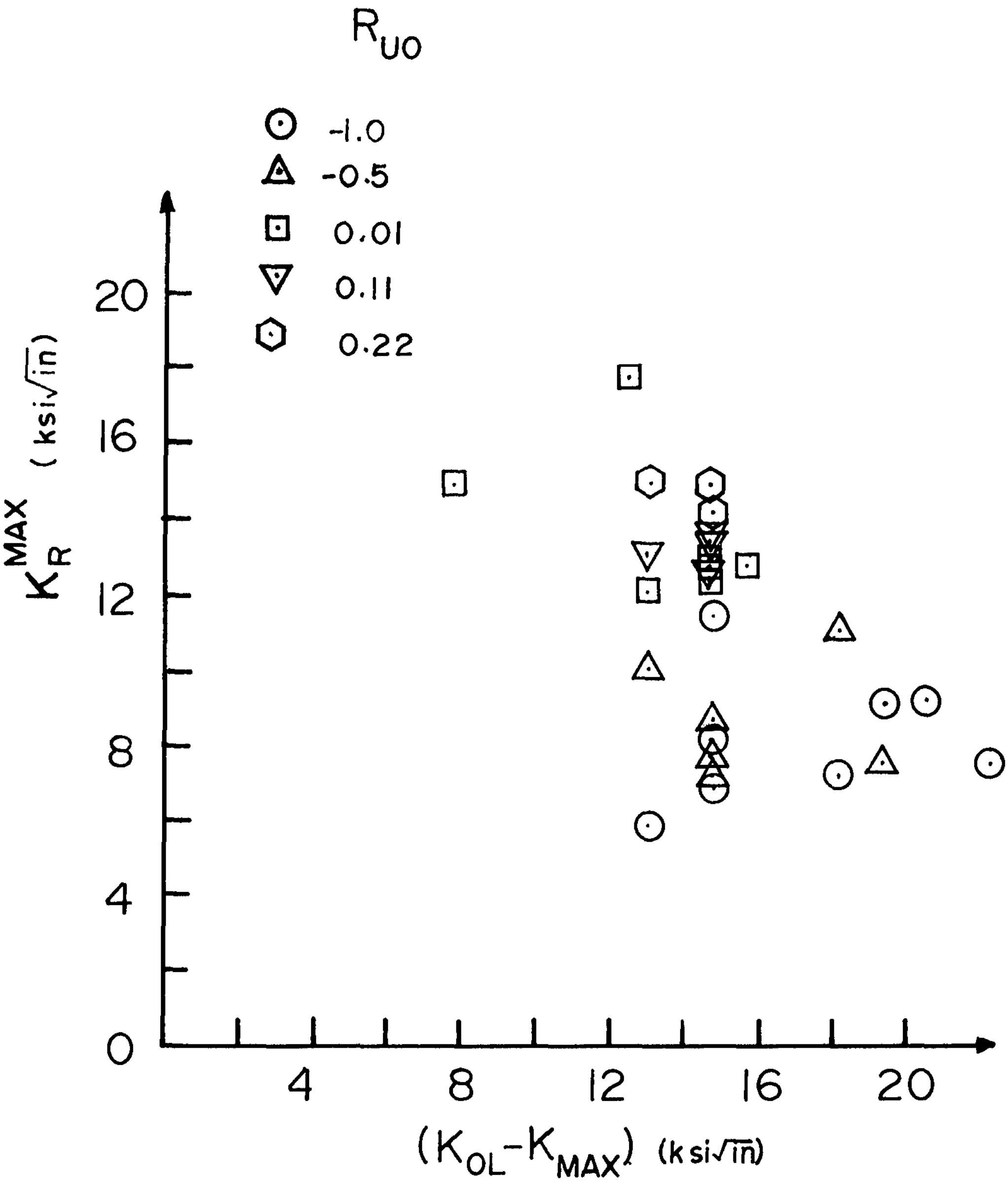

Figure 20. Comparison of maximum residual stress intensity with the Willenborg parameter, K_{OL} - K_{MAX}.

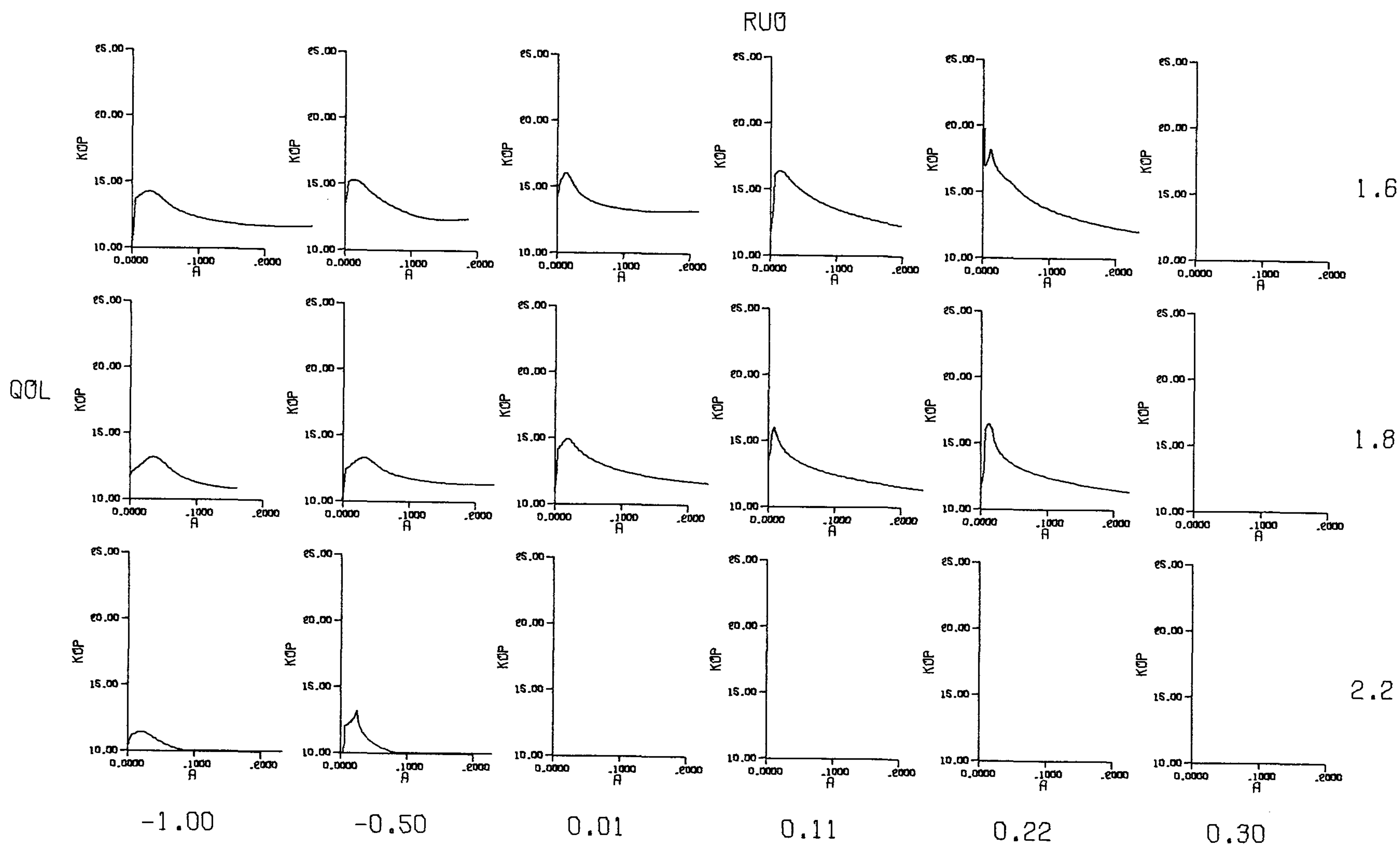

Figure 21. K_{OP} vs. a for tests in the Q_{OL} vs. R_{UO} plane (K_{MIN} = 7.33 ksi$\sqrt{in}$)

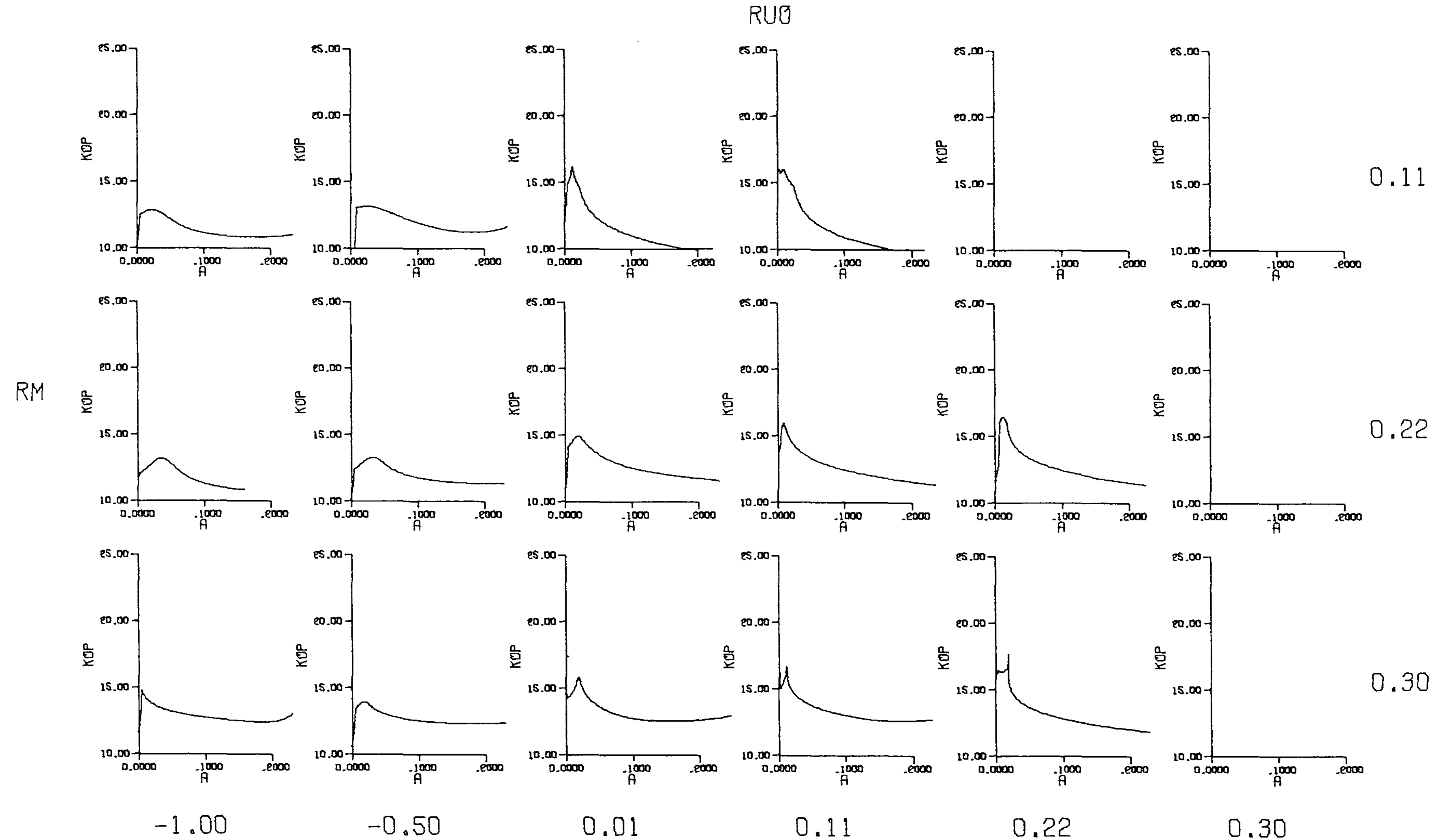

Figure 22. K_{OP} vs. a for tests in the R_M vs. R_{UO} plane (K_{MAX} = 18.52 ksi$\sqrt{in}$)

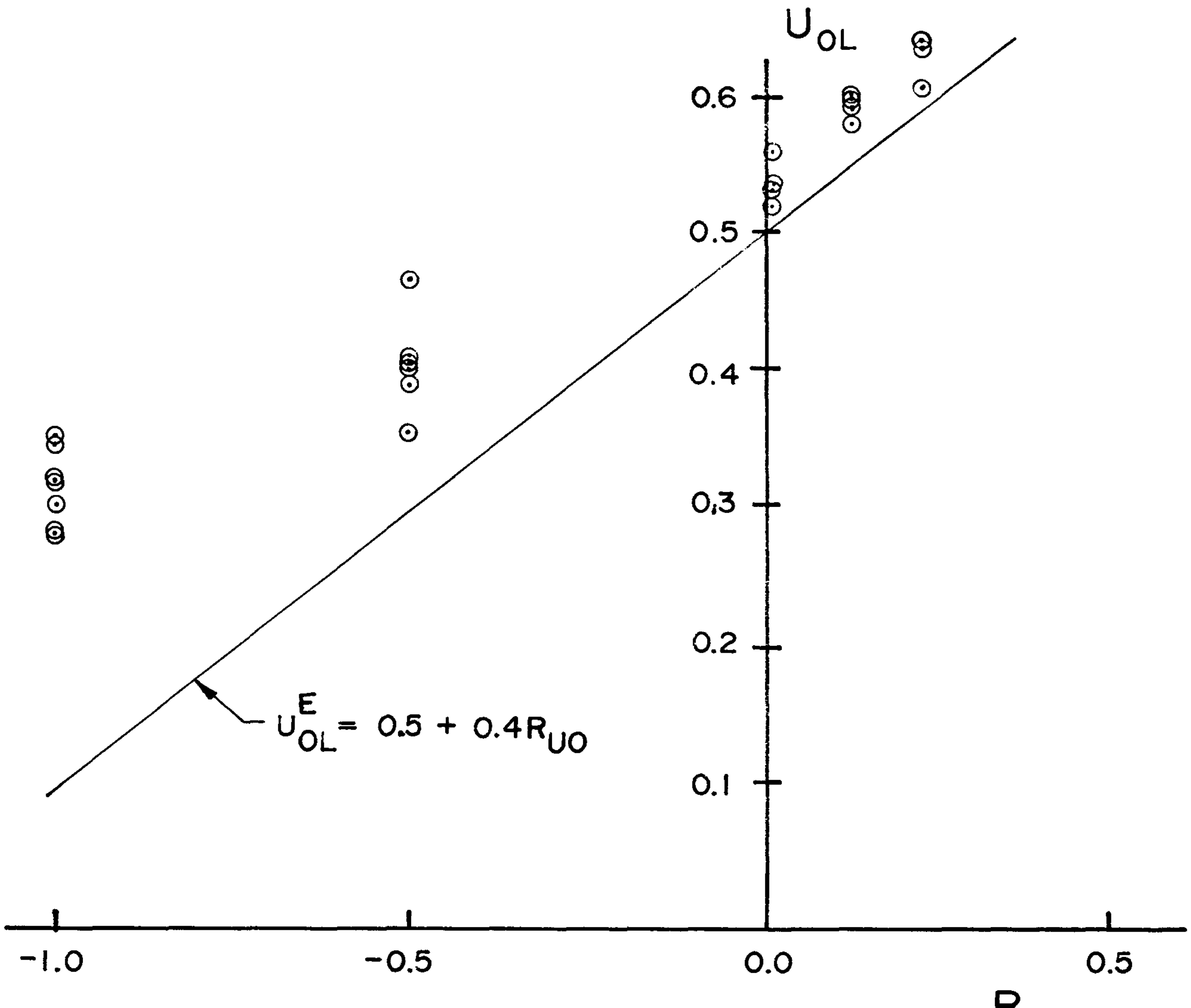

Figure 23. U_{OL} showing the direct analogy to crack closure without load interactions

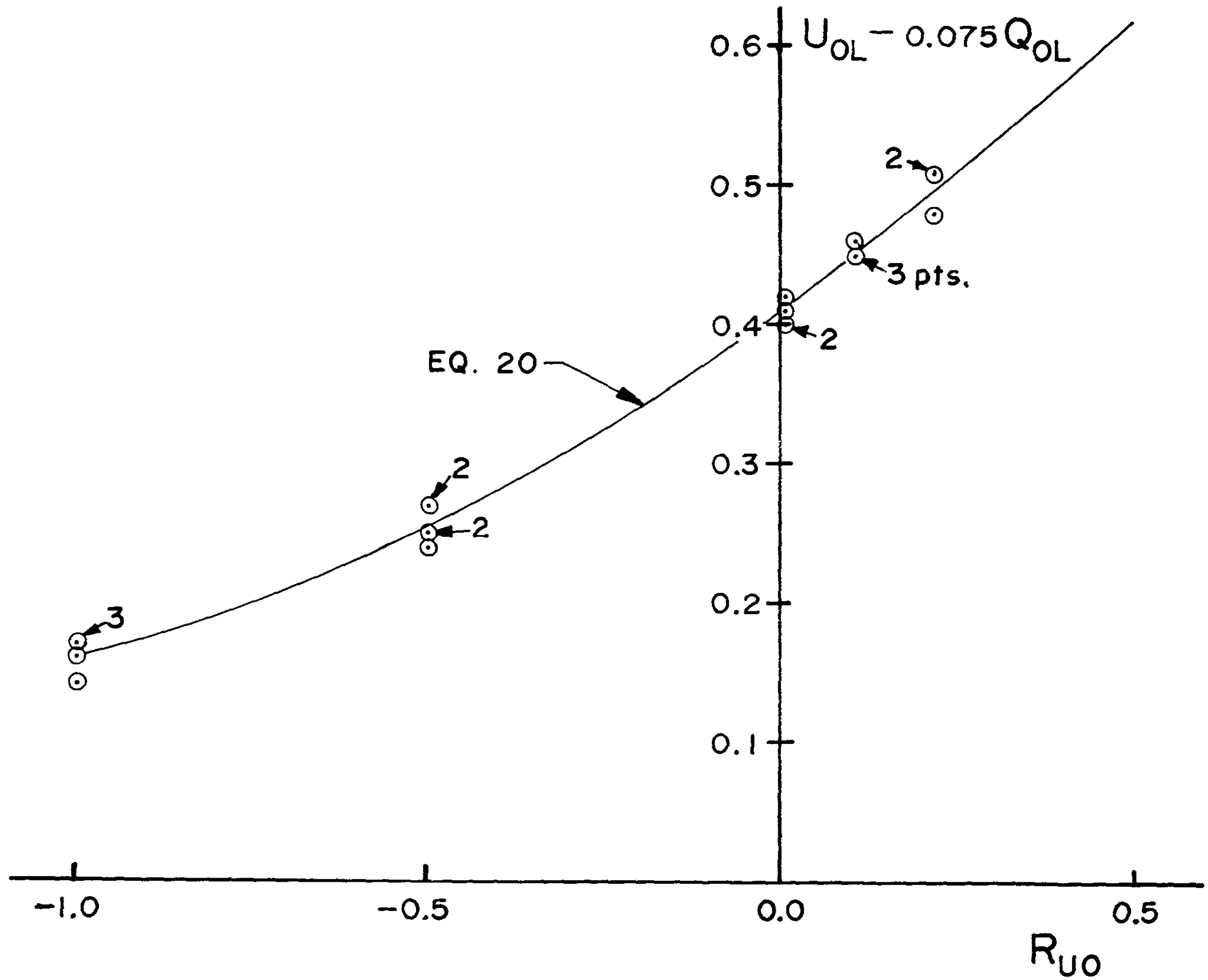

Figure 24. $U_{OL} - C_4Q_{OL}$ vs. R_{UO}

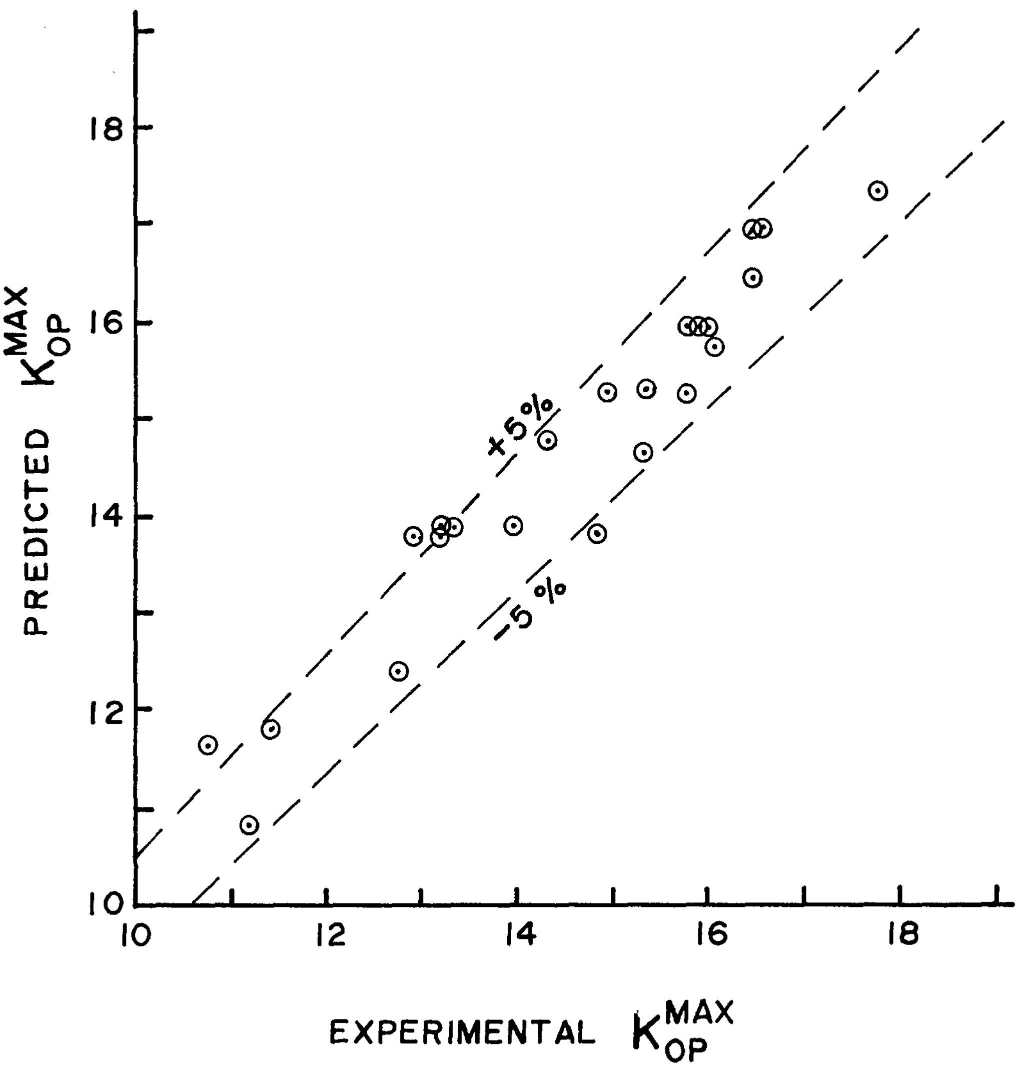

Figure 25. Comparison of predicted and experimental values of K_{OP}^{MAX}

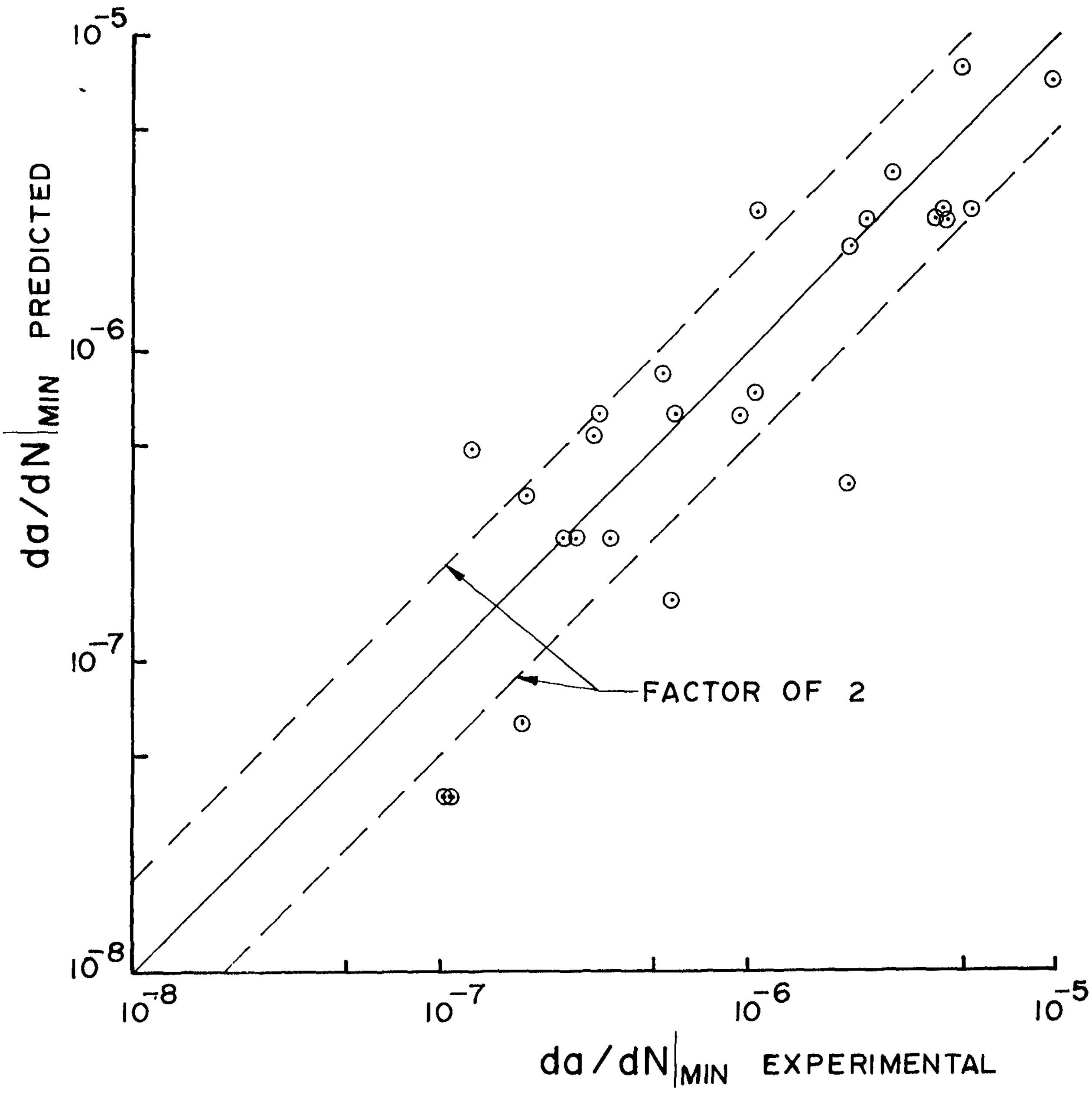

Figure 26. Comparison of predicted and experimental values of $\left.\frac{da}{dN}\right|_{MIN}$

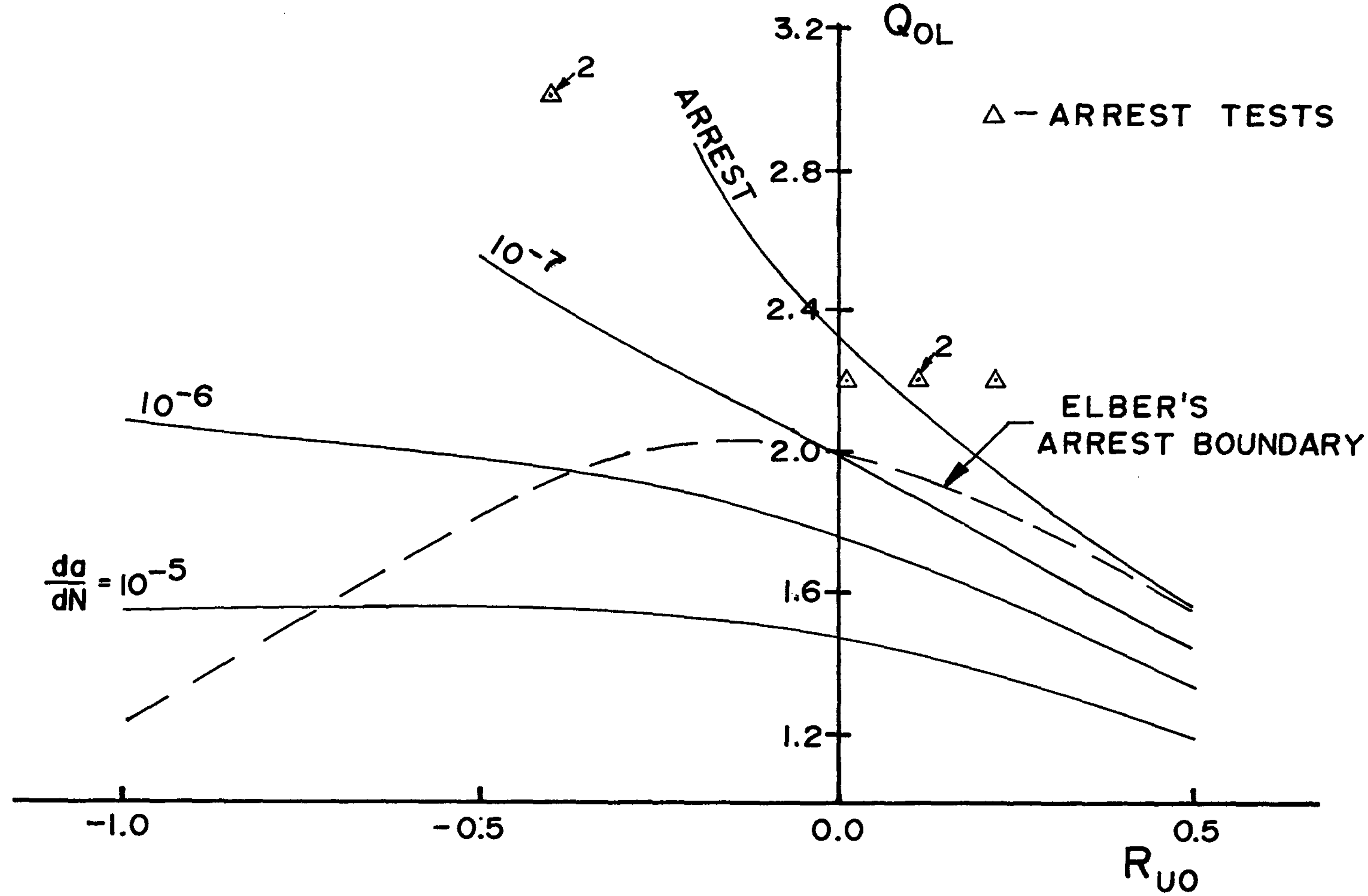

Figure 27. Curves of constant $\left.\frac{da}{dN}\right|_{MIN}$

(K_{OL} = 33.33 ksi$\sqrt{in}$)

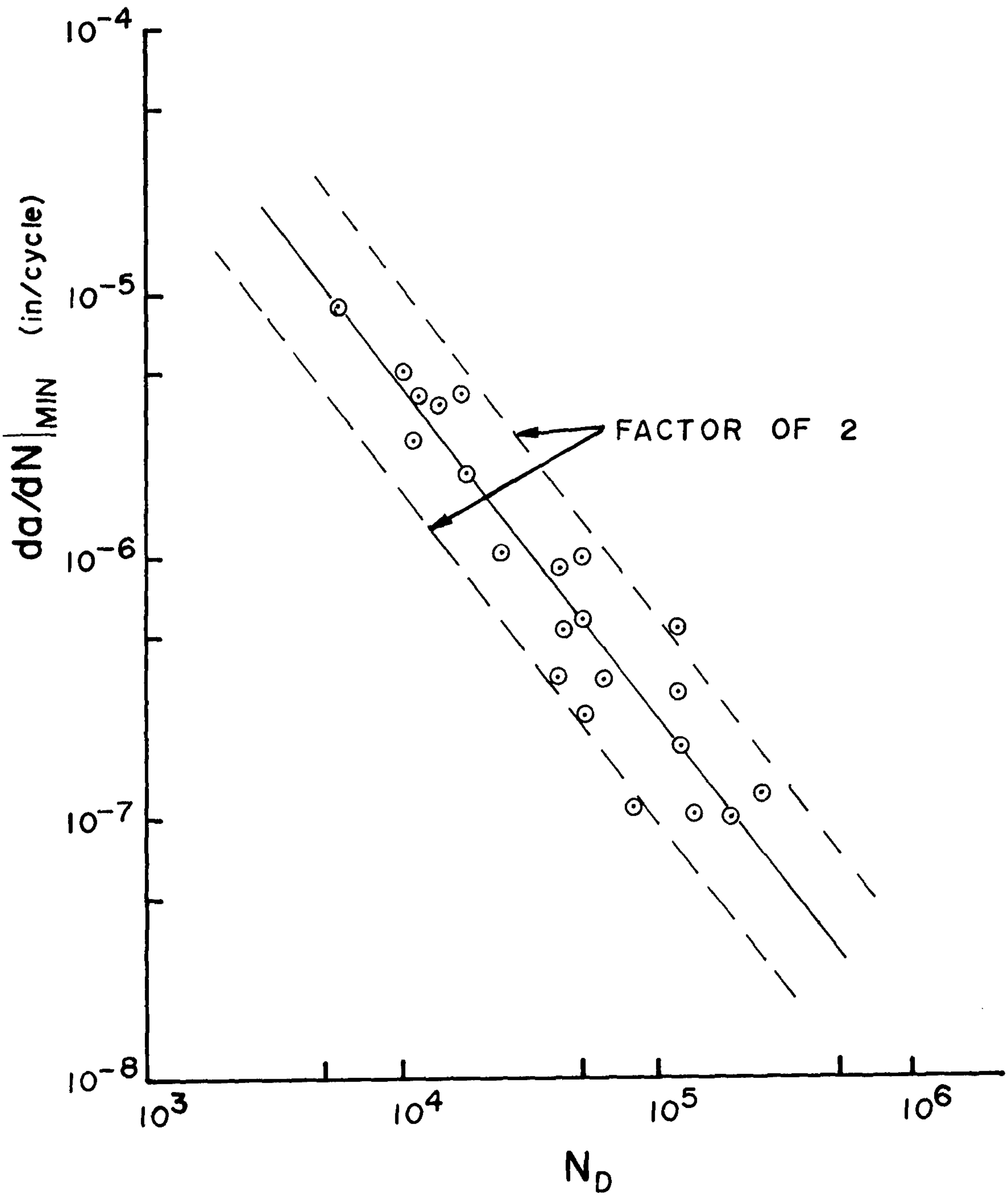

Figure 28. Minimum growth rate following overload/underload cycle versus the number of delay cycles.

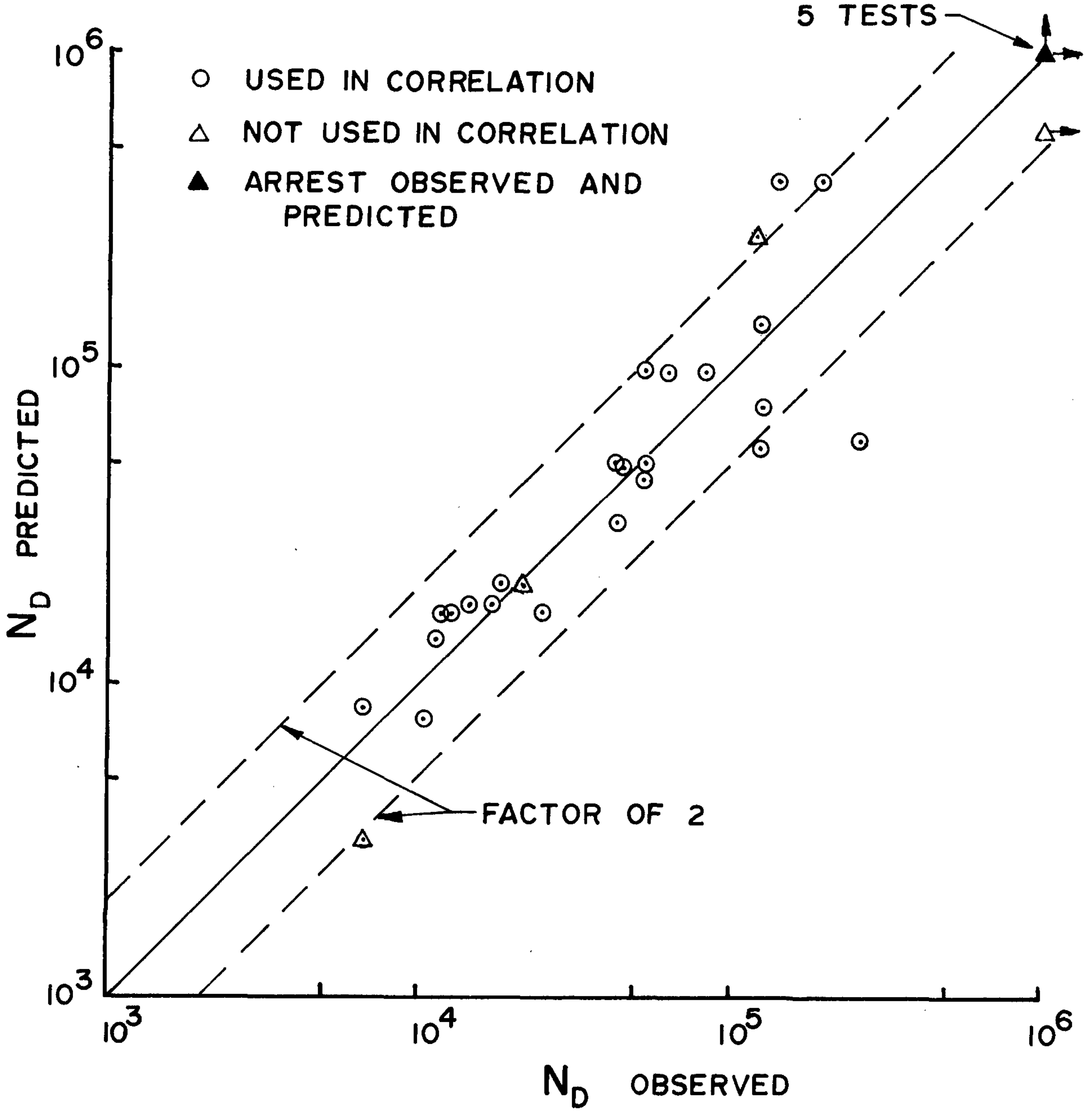

Figure 29. Comparison of predicted and experimental values of N_D

☆ U. S. GOVERNMENT PRINTING OFFICE: 1975 — 657-630/258